Research Paper

PAIN 167 (2026) 2391–2407

PAIN®

Deep FLASH-seq profiling of purified canine sensory neurons uncovers species-specific signatures relevant to pain and itch

Paula Ledesma Fernandez[a,b], Brandi Butler[b], Heidi Theis[c], Stefan Paulusch[c], Elena De Domenico[c], Greg A. Weir[a], Andrew M. Bell[a,b,*]

Abstract

Naturally occurring pain and itch disorders in the domestic dog represent an important and underexploited opportunity for translational sensory neuroscience. These conditions largely mirror human disease, highlighting the need for detailed comparative understanding of canine somatosensory neurobiology. Here, we present a single-cell transcriptomic characterisation of the canine dorsal root ganglion (DRG), providing molecular insights into sensory neuron diversity in a species of direct veterinary and biomedical relevance. We develop a novel mechanical dissociation and fluorescence-activated cell sorting strategy enabling purification of intact whole neurons from adult canine DRG, followed by deep, full-length RNA sequencing using FLASH-seq. This approach yields high-quality transcriptional profiles with molecular depth analogous to deep neuronal profiling in human DRG, enabling resolution of neuronal identities and subtype-specific gene programs. Using these data, we identify canine sensory neuron clusters conforming to conserved principles of DRG molecular organization observed across species, including peptidergic and noncanonical peptidergic nociceptors, low-threshold mechanoreceptors, proprioceptors, and thermosensory populations. Cross-species comparisons with human and mouse DRG datasets reveal broad conservation of pain- and itch-relevant pathways and therapeutic targets, alongside biologically meaningful divergence. We further identify species-specific differences in subtype-restricted expression of the pharmacologically relevant receptors *IL31RA* and *SSTR2*, which we validate using in situ hybridization and contextualize with human spatial transcriptomic data. Finally, we provide evidence that domestication-associated genes are nonrandomly enriched in specific sensory neurons, suggesting that evolutionary history may have shaped somatosensory function. These data represent a resource for comparative sensory neuroscience and inform translational interpretation of pain and itch therapeutics across species.

Keywords: Canine, Dorsal root ganglion, Single-cell, FLASH-seq, Pain, Itch

1. Introduction

The development of novel therapeutics for pain and itch has been hampered by a marked failure to translate promising preclinical analgesic candidates from rodent models.[21,65] Because naturally occurring disease in the pet dog mirrors many aspects of the human condition with greater validity than rodent preclinical models, it has been suggested that studying spontaneous painful disease in companion animals can facilitate the development of therapies for humans while also enhancing veterinary care.[2,44]

Pain and itch in dogs are, in many respects, highly similar to pain and itch in humans.[36,42,48] In both species, these sensations arise from naturally occurring conditions such as osteoarthritis and atopic dermatitis. In the domestic dog, these conditions are common, with estimated prevalences of 20%[48] and 3 to 15%,[24] respectively.

Beyond face validity, canine diseases also offer translational advantages. Time courses more closely resemble human chronicity, typically persisting for months or years rather than the shorter durations of many rodent models. Companion animals share important environmental exposures with humans, and many major treatment modalities are shared, with comparable pharmacokinetics and dosing intervals. In addition, pain and itch can be measured using a broad suite of outcome tools that extend beyond reflex-based hypersensitivity,[34,43] including validated owner-completed behavioural tools, activity and sleep metrics, and quality-of-life instruments.[17,49] However, to use the dog successfully as a translational species requires an in-depth understanding of the fundamental similarities and differences in the molecular basis of somatosensation and pain.

The ability to detect pain- and itch-inducing stimuli in the periphery depends on the existence of multiple classes of primary sensory neurons, each tuned to specific stimuli. Axons of these neurons relay this information to the dorsal horn of the spinal cord by their cell bodies in the dorsal root ganglia (DRG).[7,77] Classically, the functional heterogeneity of sensory neurons has

Sponsorships or competing interests that may be relevant to content are disclosed at the end of this article.

[a] Spinal Cord Group, School of Psychology and Neuroscience, University of Glasgow, Glasgow, United Kingdom, [b] School of Biodiversity, One Health and Veterinary Medicine, University of Glasgow, Glasgow, United Kingdom, [c] Deutsches Zentrum für Neurodegenerative Erkrankungen (DZNE) e.V., PRECISE Platform for Genomics and Epigenomics at DZNE and University of Bonn, Bonn, Germany

**Corresponding author. Address: Spinal Cord Group, Sir James Black Building, University of Glasgow, University Ave, Glasgow G12 8QQ, United Kingdom. Tel.: (+44) 141 330 5848. E-mail address: andrew.bell@glasgow.ac.uk (A. M. Bell).*

Supplemental digital content is available for this article. Direct URL citations appear in the printed text and are provided in the HTML and PDF versions of this article on the journal's Web site (www.painjournalonline.com).

© 2026 International Association for the Study of Pain

http://dx.doi.org/10.1097/j.pain.0000000000004102

Copyright © 2026 by the International Association for the Study of Pain. Unauthorized reproduction of this article is prohibited.

been described in terms of cell body size, degree of myelination, and electrophysiological properties.[16,72] However, in recent years, single-cell transcriptomics has revolutionised our understanding of the molecular basis of sensory neuron function. Across rodent,[32,51,56,60,61,67,78,86] primate,[40,47] and human datasets,[11,52,57,75,85] single-cell atlases resolve conserved DRG neuron classes and a shared nociceptor taxonomy, alongside species-specific adaptations across subtypes.[10,40]

Sensory neurons are compelling therapeutic targets,[9] with some novel approaches already used commonly or in development (eg, monoclonal antibodies targeting nerve growth factor (NGF)[13,25] and interleukin (IL)-31[64,79] signalling, and inhibitors of the Nav1.8 sodium channel) and growing interest in nociceptor-targeted chemogenetic approaches.[9,59,83] However, despite rapid advances in our understanding of rodent and human sensory neuron biology, the molecular architecture of the canine DRG (cDRG) remains comparatively underdefined.[35] This gap limits both the rational deployment of emerging therapies in veterinary patients and the translational value of the dog for chronic pain and itch.

Here, using a novel cell-sorting technique combined with FLASH-seq, a rapid full-length single-cell RNA sequencing method,[30] we demonstrate that high-quality whole-cell transcriptomic profiling of neurons from flash-frozen postmortem tissue is feasible. We then generate a single-cell transcriptomic atlas of cDRG neurons, describing canine sensory neuron populations and cross-species similarities, thereby establishing a framework for translation of pain and itch therapeutics.

2. Methods

2.1. Dorsal root ganglia collection

All experiments were approved by the Ethics committee of the School of Biodiversity, One Health and Veterinary Medicine, University of Glasgow (ref EA46/24). Tissue was acquired from 2 groups of dogs. Nonbeagle dogs (SSPCA, Glasgow, United Kingdom) were euthanized for behavioural reasons; beagle dogs (Charles River Laboratories, Tranent, United Kingdom) were part of control groups in research studies unrelated to pain.

Dogs were humanely euthanised with an overdose of barbiturates, and DRGs were collected from the lumbar area within 2 hours from death. Dorsal root ganglia collected for single-cell sequencing and in situ hybridization were immediately flash frozen on dry ice and stored at −80˚C. Dorsal root ganglia used for immunohistochemistry were immersion fixed in 4% paraformaldehyde for 48 hours, cryoprotected in 30% sucrose, and stored at −150˚C.

2.2. Immunohistochemistry

Ganglia were trimmed to remove adjacent nerve roots and connective tissue and embedded in 4% agar. Sixty-micrometer-thick transverse sections were cut with a vibrating blade microtome (Leica VT1200; Leica Microsystems, Wetzlar, Germany) and nonsequential (1:2) sections were used for downstream experiments. Immunohistochemical reactions were performed on free-floating sections. To measure neuronal diameter, NeuN antibody (clone EPR12763, Catalog N˚ ab190565; Abcam, Cambridge, United Kingdom) was used for neuronal cytoplasm and nuclei identification. Use of this antibody has not been previously reported in canine dorsal root ganglia; however, the same clone is manufacturer-validated for canine brain and spinal cord tissues, is listed as reactive in dog in immunohistochemical applications, and recognises neurons in canine cortex.[8] Sections were incubated overnight with conjugated antibody NeuN-647 (rabbit, 1:1000) at 4˚C in phosphate-buffered saline (PBS) that contained 0.3 M NaCl, 0.3% Triton X-100, and 5% normal donkey serum. After immunoreaction, sections were rinsed for 5 minutes with PBS double salt before incubation in Hoechst (1:1000 in PBS) for 15 minutes, then rinsed for 5 minutes with PBS double salt. Sections were mounted in anti-fade medium and stored at −20˚C.

Sections were scanned with a Zeiss 710 LSM confocal microscope (Carl Zeiss Microscopy GmbH, Jena, Germany) (Argon multi-line, 405 nm diode, 561 nm solid state), using ×20 objectives (NA 1.2), at 1 Airy Unit. Two-micrometer z-step images of the whole thickness of the section were obtained.

2.3. Measurement of neuronal diameter

For the analysis of neuronal diameter, we examined transverse sections from the DRG of each animal. We used Neurolucida (version 2021.1.3; MBF Bioscience, Williston, VT, USA) to measure neuronal area. To minimise selection bias, images were overlayed with a 160 ×160-μm grid and the neuron closer to the upper left corner of each grid square was selected for analysis. Only NeuN-647 positive neurons with visible margins and nuclei included in the section were measured. To ensure that a total of 100 neurons were analysed per section, grid squares sizes were adjusted according to the total area of DRG section. To calculate neuronal diameter, data were transferred to Microsoft Excel (Microsoft Corporation, Redmond, WA, USA) and subsequently analysed in R (version 4.3.1) for graphical representation.

2.4. Measurement of non-neuronal cell: neuronal cell ratio

For the analysis of the non-neuronal to neuronal cell ratio, the central focal plane of the immunohistochemical scans was selected and used for counting. Analysis was performed in Qupath (version 0.6.0).[5] Neuronal nuclei were identified as Hoechst-positive and NeuN-647-positive, whereas non-neuronal nuclei were identified as Hoechst-positive and NeuN-647-negative.

2.5. RNA quality assessment

Ten-micrometer-thick sections of DRG tissue were collected using a cryostat (Leica CM1950; Leica Microsystems, Wetzlar, Germany), homogenized, and processed for RNA extraction according to the standard RNeasy Micro-Qiagen protocol for RNA extraction from animal cells (Qiagen, Hilden, Germany). RNA quality was assessed with RNA Integrity Number measured by Agilent 2100 Bioanalyzer (Agilent Technologies, Santa Clara, CA, USA).

2.6. Cell dissociation

Dorsal root ganglia dissociation followed a described protocol with modifications.[63] Before dissociation, all buffers and tubes were prechilled on ice. Briefly, DRGs were processed separately for each dog, such that each cell suspension corresponded to 1 individual animal (2-3 DRGs per dog). Dorsal root ganglia were placed in a petri dish on ice with 1 mL of twin-salt-tris (TST) buffer. Surrounding roots and connective tissue were excised. While keeping the petri dish on ice, DRGs were minced with McPherson Vannas Scissors 45˚ angled (Fine Science Tools GmbH, Heidelberg, Germany) and then Noyes Spring Scissors (Fine Science Tools GmbH) for 30 seconds.

Copyright © 2026 by the International Association for the Study of Pain. Unauthorized reproduction of this article is prohibited.

To assess neuronal cell integrity and tissue dissociation, the minced DRGs were observed under a microscope. Mincing was repeated for the minimum time required to achieve full DRG dissociation. After this, dissociation continued with fired-polished pipettes of decreasing diameter until a single-cell suspension containing neuronal cells was obtained. The resulting cell suspension was filtered through a 150-μm strainer (pluriSelect Life Science, Leipzig, Germany) into a 15-mL Falcon tube. Remaining cells in the petri dish were collected with an additional 1 mL of TST and passed through the same filter, followed by 3 mL of salt-tris buffer (ST). The filtered suspension was centrifuged at 4˚C (500*g*, 5 minutes).

The resulting pellet from each donor was resuspended in PBS containing 2% bovine serum albumin (BSA) and incubated for 30 minutes at 4˚C with conjugated NeuN-647 (ab190565; Abcam) added at a final dilution of 1:500. After incubation, samples were rinsed twice in PBS containing 2% BSA at 4˚C. The final pellet was resuspended in PBS containing 0.04% BSA. To assess cell integrity, 10 μL was taken and mixed with SytoxGreen (Catalog N˚ S7020; Thermo Fisher Scientific, 1:1000) and visualised on an epifluorescence microscope before fluorescence-activated cell sorting (FACS).

2.7. Cell sorting

Before sorting, a colorimetric plate calibration was used as previously described.[62] Sorting was performed using a 130-μm nozzle and Eppendorf twin.tec PCR Plate 384 LoBind plates (Eppendorf, Hamburg, Germany). Neuronal cells (Sytox Green-positive/NeuN-647-positive) were sorted using a BD FACSAria IIU Flow Cytometer (BD Biosciences, Franklin Lakes, NJ, USA) equipped with 4 laser (405, 488, 561, and 633 nm) and a 130-μm nozzle. Sytox Green emissions were detected using a 530/30BP, 502LP, and anti-NeuN-APC emissions using a 670/14 BP filter. The 2-colour flow cytometric analysis was performed using BD FACSDiva Software (version 8.0.1; BD Biosciences) on Microsoft Windows 7 operating system. At the start of each sorting session, unstained samples were used to verify gating.

Cells were sorted into 384-well plates containing FLASH-seq lysis buffer.[30] Each plate was sex-balanced during sorting, such as that half of the plate contained neuronal cells from a male and the other half cells from a female donor. Plates were centrifuged before sorting (500*g*, 1 minute) and were maintained at 4˚C throughout FACS. After sorting, plates were sealed, centrifuged (500*g*, 1 minute) and snap-frozen on dry ice and stored at −80˚C until further processing.

2.8. Sequencing and alignment

The trial plate was processed and sequenced independently. The 4 final plates were processed in parallel. Single-cell RNA-seq libraries were generated using the FLASH-seq protocol with minor modifications.[30]

After cells sorting directly into 384-well plates containing lysis buffer supplied with dNTPs, SMART-dT30VN primer, dCTP, and FlashSeq-Template Switching Oligo (FS-TSO), the plates were snap-frozen and stored at −80˚C until further processing. Reverse transcription polymerase chain reaction (RT-PCR) was performed by adding 4 μL of RT-PCR mix containing Superscript IV (Thermo Fisher Scientific, Waltham, MA, USA) to each well using the I.DOT Non Contact dispenser (Dispendix, Heidelburg, Germany). The RT reaction was conducted at 50˚C for 60 minutes followed by a pre-amplification PCR of 21 cycles. Amplified products were purified using the C.WASH noncontact centrifugal plate washer (CYTENA, Freiburg im Breisgau, Germany) for the beads clean up step.

To normalize the libraries, nuclease-free water was added to achieve a final average concentration of 200 pg/μL. Subsequently, 0.5 μL of cDNA underwent tagmentation and enrichment using the Tagmentase (Tn5 transposase)—unloaded (Diagenode). Quantification of the final libraries was performed using the Qubit HS dsDNA assay, and the fragment size distribution was measured using HS D1000 assay on an Agilent TapeStation 4200 system.

Sequencing was performed in paired-end mode (PE75) on a NovaSeq X Plus systems (Illumina, San Diego, CA, USA) using NovaSeq X Series 10B Reagent Kit chemistry. Raw sequencing data were demultiplexed using bcl2fastq2 v2.20. Read quality was assessed using FastQC v0.11.9 and MultiQC v1.14. Reads were aligned against the C. lupus reference genome (Ensembl 108) using Kallisto v0.48.0. The alignment pipeline was managed using Snakemake v7.20.0.

2.9. Analysis of single-cell RNA seq data

R (version 4.3.1) and Seurat (version 5.4.0) were used for the single-cell RNA-seq analysis. One Seurat object was generated per plate (5 objects in total).

2.10. Preliminary analyses to determine Quality Control (QC) thresholds and batch correction strategy

Initial inspection of the data revealed differences in the number of detected unique genes per cell (nFeature_RNA) between sexes, which drove significant cluster differences in un-batch corrected Uniform Manifold Approximation and Projection (UMAP) plots. To determine whether these differences reflected technical artifact or differences in sorted cell composition (ie, neuronal vs non-neuronal cells), datasets were first analysed separately by sex and no quality control thresholds (ie, nFeature_RNA or nCount_RNA) were used.

Within each sex, layers were split by individual, to mitigate interindividual batch effect. Data were first normalized (NormalizeData), highly variable features were identified (Find Variables Features), scaled (ScaleData), and subjected to Principal Component Analysis (RunPCA). To correct for dog-specific batch effects, datasets within each sex were integrated using canonical correlation analysis (CCA) (Integrate Layers, method = CCA Integration, origi.reduction = "pca," new.reduction = "integrated.cca," assay = "RNA," verbose = FALSE). Clustering was performed using FindNeighbors (reduction = "integrated.cca," dims = 1:30), FindClusters (resolution = 0.5, cluster.name = "cca_clusters"), and RunUMAP (reduction = "integrated.cca," dims = 1:30, reduction.name = "umap.cca").

To compare cell-type composition between sexes, clusters were annotated into broad cellular classes using a marker gene list formed by canonical markers to distinguish neurons large and small diameter and non-neuronal (GFAP-positive) cells (marker_map <- list (Non_neurons = "*GFAP*," Neurons = c ("*UCHL1*," "*TUBB3*")), Large = c ("*NEFH*," "*NTRK2*," "*PIEZO2*," "*NTRK2*," "*PIEZO2*," "*NTRK3*," "*PVALB*"), Small=c ("*INA*," "*SCN10A*," "*PRDM12*," "*NTRK1*," "*TRPV1*," "*SST*," "*CALCA*," "*MRGPRD*," "*VGLUT3*," "*TRPM8*")). Comparison of annotated datasets showed similar proportions of neuronal vs non-neuronal cell populations between sexes, supporting nFeature_RNA differences were not caused by cell-composition and supporting subsequent preliminary joint analysis. A nondefined cluster characterised by uniformly low gene detection was labelled "Low" and excluded.

Copyright © 2026 by the International Association for the Study of Pain. Unauthorized reproduction of this article is prohibited.

Male and female datasets were then merged into a single Seurat object. Inspection of the merged dataset identified an additional cluster characterised by reduced nFeature_RNA and increased mitochondrial transcript abundance. All cells in this undefined additional "low" cluster were removed using a nFeature_RNA threshold of 1250, and this was carried forward for final analysis.

2.11. Final processing, integration, and clustering

The filtered dataset (subset [subset = nFeature_RNA ≥ 1250]) was renormalized (NormalizeData), and 3000 variable features were selected (Find Variables Features, nfeatures = 3000). Data were scaled (ScaleData) and subjected to Principal Component Analysis (RunPCA). Then layers were integrated using CCA, using dog as the integration variable (IntegrateLayers [method = CCAIntegration, orig.reduction = "pca," new.reduction = "integrated.cca," verbose = FALSE, k.weight=72]; FindNeighbors [reduction = "integrated.cca," dims = 1:30]); followed by final clustering (FindClusters [resolution = 1.5, cluster.name = "cca_clusters"]) and dimensionality reduction RunUMAP(reduction = "integrated.cca," dims = 1:30, reduction.name = "umap.cca").

Violin plots and FeaturePlot UMAPs were generated in Seurat to illustrate the distribution of selected genes across clusters. Unbiased marker genes for each cluster were identified using the Wilcoxon rank sum test (FindMarkers) and filtered for avg_log2FC > 1 and adjusted *P* value < 0.05; the top 5 markers per cluster were selected based on adjusted *P* value and log2 fold change. Myelination index for each cluster was generated based on an aggregated expression score (AddModuleScore) of myelin associated genes (*NEFH*, *NEFM*, *SCN8A*, *NFASC*, *KCNQ2*, *KCNQ3*, *KCNA1*, and *CNTN1*).

2.12. Cross-species analysis

Mouse[67] and human[85] single cell/nucleus datasets were integrated with the canine dataset to enable comparisons across species. Before integration, all genes were converted to human 1:1 orthologues using the orthogene package (orthogene::convert_orthologs [method = "gprofiler," drop_nonorths = TRUE, non121_strategy = "drop_both_species"]). New Seurat objects were then reconstructed using the filtered matrices while preserving the original metadata. This ensured that all downstream integration steps were performed on a common, human-symbol gene space across dog, human, and mouse. Orthologue-mapped dog, human, and mouse objects were then merged into a single Seurat object. Standard preprocessing steps were applied: log-normalisation, identification of 3000 variable features, and scaling as described above.

For cross-species alignment, datasets were integrated using Seurat's CCA-based layer integration (IntegrateLayers [method = CCAIntegration, orig.reduction = "pca," new.reduction = "integrated.cca"]). Nearest-neighbour graphs were constructed using the integrated CCA reduction (FindNeighbors [dims = 1:30]), clusters were identified at resolution 1.2 (FindClusters [resolution = 1.2]), and UMAP embeddings were generated from the integrated space (RunUMAP [dims = 1:30]). Species-split and merged UMAPs were used to visualise cluster alignment and assess cross-species correspondence. These integrated UMAPs were used to assess cross-species correspondence among clusters and to confirm the presence of conserved neuronal types across dog, human, and mouse. After integration, clustering was re-annotated into a simplified unified cross-species set, following the rationale outlined in the Results section. This approach allowed direct comparison of homologous sensory neuron classes.

To characterise molecular features that were shared or divergent across species, we performed cluster-wise differential expression analyses on the orthologue-mapped, integrated dataset. To focus analyses on physiologically and pharmacologically relevant gene families, we additionally generated curated gene lists representing ion channels, G-protein coupled receptors (GPCRs), synaptic proteins, transcription factors, and neuropeptides (sourced from published datasets).[15,31,73,76] These lists were harmonised and used to define a focus gene set.

Before marker testing, we applied cross-species detectability filters to minimise artefacts arising from sparse counts or uneven species representation. For each gene, we computed the proportion of cells with detectable expression (>0 in the "data" slot) within dog, human, and mouse subsets. Genes were retained only if they were detected in at least 2% of cells in *each* species overall and were detected in at least 1 species outside the focal cluster (>2% detection, ie, globally detectable somewhere to reduce the potential for sparse potentially artifactual expression dominating results). Conserved markers were identified within each unified cross-species cluster using Seurat's FindConservedMarkers (FindConservedMarkers, test.use = "wilcox," only.pos = TRUE). Genes were required to have a positive log2 fold-change ≥0.25, expression in ≥10% of cells in the focal cluster, and species-wise adjusted $P < 0.05$. Conserved genes were ranked according to the maximum adjusted *P*-value across the 3 species, and the top 20 markers per cluster were visualised using dot plots with species as the grouping variable (DotPlot). Divergent, species-biased markers were identified using 3 pairwise contrasts within each cluster (Dog vs Human, Dog vs Mouse, Human vs Mouse) using FindMarkers (FindMarkers, logfc.threshold = 0.25, min.pct = 0.10, test.use = "wilcox"). Genes meeting an adjusted *P*-value threshold <0.05 in any pairwise test were considered divergent for that species pair. For visualisation, the most strongly differentially expressed genes (top 20 by absolute log2 fold-change) were summarised in dot plots for each contrast. To quantify convergence and divergence across species, significant gene sets were partitioned into intersection categories (Human-only, Dog-only, Mouse-only, Human–Dog, Human–Mouse, Dog–Mouse, and Human–Dog–Mouse). Area-scaled Euler diagrams were generated using the eulerr package, based on the species-specific significance sets after applying all statistical and detectability filters. These diagrams represent the strict convergence of genes that are significantly enriched in the same cluster across all 3 species, which is more restrictive than the ranked top-20 conserved lists used for visualisation.

2.13. Expression of domestication selected genes in canine dorsal root ganglia

To test whether domestication-associated genes were non-randomly distributed across canine sensory neuron subtypes, we performed an enrichment analysis using a published list of positively selected genes (PSGs) identified in genome-wide domestication scans of dogs.[89] All analyses used PSGs that were detectably expressed within the dataset.

Genes expressed in at least 3 cells across the full cDRG dataset defined the background set (sum of non-zero counts ≥ 3). Differentially expressed genes (DEGs) were identified for each transcriptional cluster using Seurat's FindMarkers (only.pos = TRUE, min.pct = 0.1, logfc.threshold = 0.25), and DEGs with

Copyright © 2026 by the International Association for the Study of Pain. Unauthorized reproduction of this article is prohibited.

$P_val < 0.001$ were retained. For each cluster, we tested whether PSGs were overrepresented among DEGs using the upper-tail hypergeometric distribution. Here, X denotes the number of PSGs obtained when sampling n genes at random from the background set, allowing us to evaluate whether the observed overlap (k) exceeds that expected by chance. The enrichment probability was:

$$P = \Pr(X \geq k) = phyper(k-1, K, N-K, n, lowertail = FALSE)$$

where N = total number of background genes, K = number of background genes that were PSGs, n = number of DEGs for a given cluster, k = number of PSGs among those DEGs. *P*-values were corrected for multiple testing across all 13 clusters using the Benjamini–Hochberg false discovery rate (reported as *q*). This provided cluster-wise inference while controlling for global multiplicity.

To validate enrichments against a data-driven null, we performed 1000 permutation tests per cluster. At each iteration: n genes were sampled uniformly at random from the background (preserving the observed cluster-specific DEG set size), the number of PSGs in the random sample was counted, and this distribution of random overlaps was compared to k, the observed overlap. The permutation *P*-value was computed as:

$$P_{\text{perm}} = \frac{\{\text{draws with overlap} \geq k\}}{1000}$$

Clusters with 0/1000 permutations meeting or exceeding the observed value were reported as *<1.00e−3*.

2.14. Integration with canine 10× data

Data from FLASH-seq experiments was integrated with independently generated 10× Chromium canine DRG data to generate a high transcriptional coverage atlas. For methods related to this, please see the companion paper.[39]

2.15. Fluorescent in situ hybridization

Lumbar DRGs from Beagles were obtained as described above. Surrounding nerves and connective tissue were removed. A DRG from each dog was drop-fixed in paraformaldehyde 4% for 13 to 16 hours, embedded in Optimal cutting temperature compound (OCT), and sectioned at 16 μm thickness using a cryostat (Leica CM1950; Leica Microsystems). Nonsequential sections were mounted onto Superfrost plus glass slides (Epredia, Portsmouth, NH, USA), with 1 slide prepared per animal.

Fluorescent in situ hybridization was performed using HCR Gold RNA-FISH kit (Molecular Instruments) according to the manufacturer's protocol for slide-mounted samples. Slides were sequentially dehydrated in 50%, 70%, and 100% ethanol (5, 5, and 10 minutes, respectively) at room temperature, air dried, and each section group encircled using a hydrophobic pen (Hydrophobic Barrier Pen; Invitrogen, Carlsbad, CA, USA). Slides were then placed in a warm humidified chamber and incubated in Hifi Probe Hybridization Buffer at 37°C for 10 minutes.

All probe sets were designed against dog (*Canis lupus familiaris*) mRNA sequences (Table S1, https://links.lww.com/PAIN/C563). Probe sets were diluted 1:50 in Hifi Probe Hybridization buffer and applied to sections for overnight incubation at 37°C. Channel allocation varied between experiments (Table S1, https://links.lww.com/PAIN/C563). After hybridization, slides were rinsed 4 times for 15 minutes each in 1× HiFi Probe Wash Buffer at 37°C. Sections were then incubated in HCR Gold Amplifier Buffer at room temperature for 30 minutes before hairpin application. Corresponding hairpin amplifiers (Table S1, https://links.lww.com/PAIN/C563) were snap-cooled, diluted 1:50 in HCR Gold Amplifier Buffer, and applied to the sections for overnight incubation at room temperature in the humidified chamber in the dark. After amplification, slides were washed 4 times for 15 minutes in 1× HCR Gold Amplifier Wash Buffer. Nuclei were counterstained with 4′,6-Diamidino-2-Phenylindole (DAPI 1:1000) in 5× Saline Sodium Citrate (Invitrogen; Cat no. 15557-044) for 1 minute. Slides were rinsed, air dried, and cover-slipped with mounting medium. Slides were stored at −20°C until imaging.

Dorsal root ganglia sections were imaged on a Zeiss LSM 900 confocal microscope (Carl Zeiss Microscopy GmbH) (405, 488, 561, and 640 nm diode) using a ×40 magnification objective (NA 1.3) in Airyscan Mode. Laser channels selected to scan sections were chosen according to the Alexa Fluor channels selected for each probe, and for DAPI, in addition, 488-nm channel was used in all scans to detect autofluorescence arising from lipofuscin within neuronal cell bodies because it mimics true in situ signal.[66]

One focal plane was acquired for each DRG section. To ensure sufficient sampling (at least 100 neurons per dog), at least 3 sections were imaged per dog. The sections imaged were selected at random, but preference was given to sections free of sectioning artifact.

2.16. Analysis of in situ hybridisation images

Airyscan raw image files were processed and stitched using Zen software (Carl Zeiss Microscopy GmbH), and individual images were generated for each section. Images were opened in QuPath (version 0.6.0). For all analyses, only neuronal cells with visible nuclei in the acquired focal plane, identified by DAPI staining, were included. Probe signal was assessed manually, using the 488 nm autofluorescence channel to identify and exclude lipofuscin-associated signal from scoring. All scoring was performed by a single observer per experiment.

Neuronal categorisation followed similar analytical workflows for both probe combinations, with channel specific modifications as described below. For analyses based on *IL31RA* expression, *IL31RA*-positive neurons were annotated initially, after which *IL31RA* annotations were masked to avoid bias during subsequent *GFRA2* identification. Co-expression was then determined by overlay of the 2 independent annotations.

For *KIT* and *SSTR2* probes, heterogeneity in signal intensity and puncta density was observed across neuronal cell bodies. Neurons were therefore classified into 3 categories: negative (no signal above background), positive (+; sparse puncta distributed across the cytoplasm without homogenous clustering), or strongly positive (++; dense, clustered puncta filling the cytoplasm with high signal intensity). Soma area was measured by manually delineating the soma boundaries; neuronal diameter was calculated assuming neuronal circular geometry of cross sections at the level of the nucleus using the equation $Diameter = \sqrt{\frac{4A}{\pi}}$.

Neurons were categorised as small (<40 μm), medium (40-60 μm), and large (>60 μm). For both analyses, neuronal measurements and classification data were transferred to Microsoft Excel (Microsoft Corporation) and subsequently analysed in R (version 4.3.1) for statistical analysis and graphical representation.

2.17. Reanalysis of Xenium in situ data

Publicly available Xenium data from Yu et al.[85] was reanalysed in Xenium explorer software (version 4.1.1; 10x Genomics,

Copyright © 2026 by the International Association for the Study of Pain. Unauthorized reproduction of this article is prohibited.

Pleasanton, CA, USA). Dorsal root ganglia sections were viewed with the DAPI channel visible. Neurons expressing >5 cytoplasmic transcripts of either *IL31RA* or *GFRA2* were marked using the annotations feature as *GFRA2*+ or *IL31RA*+. Neurons of each class were annotated separately without viewing the channel for the other transcript. Annotations were exported and colocalization calculated using custom R scripts.

3. Results

3.1. Assessment of neuronal size and neuronal vs non-neuronal cell ratio in canine dorsal root ganglia

To inform our neuronal isolation and sequencing methodologies, we first sought to define the neuronal size distribution and ratio of neurons to non-neuronal cells in cDRG. For these initial experiments, we used tissue sections from 4 dogs of mixed breeds (German Shepherd, Greyhound, XL Bully, & Border Collie), which were reacted with antibodies against NeuN and counterstained with DAPI. We observed that NeuN labelled all neuronal profiles (as recognised using DAPI staining by size, profile, and the presence of a large pale nucleus compared with non-neuronal cells, **Fig. 1A**). In contrast to reports of imperfect Hoechst/DAPI labelling of large sensory neurons in human DRG, we did not observe an increased frequency of pale or absent nuclear labelling in large neuronal profiles in cDRG (**Fig. 1B**). Using a stereological technique, we measured the size of 100 neurons per animal and found that neuronal diameter ranged from 21 to 81 μm (**Fig. 1C** and Table S2, https://links.lww.com/PAIN/C563). When compared with sizes of DRG neurons across species,[68,84] cDRG neurons seem to be of a size more akin to human than rodents. We also observed that neuronal nuclei were greatly outnumbered by non-neuronal nuclei. We quantified this in single optical sections from the same confocal images as used above, with this method chosen to allow comparisons with recently available data from human DRG (hDRG).[88] We manually counted an average of 15,549 (range 14,626-16,045) non-neuronal nuclei per animal vs 224 (194-265) neuronal nuclei. The ratio of neuronal to non-neuronal nuclei across the whole DRG section was calculated as 1:65 (range 1:56-1:75; Fig. S1, https://links.lww.com/PAIN/C563). Overall, neuronal nuclei comprised approximately 1.6% of all nuclei, closely matching reported proportions in human DRG.[88] The abundance of non-neuronal cells led us to develop a method to enrich neuronal cells for sequencing using FACS.

3.2. Dissociation of canine dorsal root ganglia and fluorescence-activated cell sorting purification of neurons for scRNA-seq

Lumbar ganglia for all FACS and sequencing experiments were acquired post-mortem from 10 laboratory beagles (6 males and 4 females, 9-24 months old) and flash frozen. These dogs were control (no drug) animals in unrelated toxicological studies and were healthy with no known painful conditions. To ensure high-quality RNA, we verified RNA integrity number (RIN) was >7.5 for each donor (Table S3, Fig. S2a, https://links.lww.com/PAIN/C563). In initial experiments, the ganglia's robust nature and connective tissue presented a challenge to dissociation. However, we found that using a dissociation protocol based on mincing and triturating tissue in Tween-based salt solution[30] could successfully dissociate the ganglia. After dissociation, we performed NeuN staining of the resultant suspension and consistently observed that whole neuronal cells, with recognisable cytoplasm and nuclei, were present alongside non-neuronal nuclei (Fig. S2c, https://links.lww.com/PAIN/C563). We purified these neuronal cells by FACS (Fig. S2b and c, https://links.lww.com/PAIN/C563), sorting cells directly into individual wells of 384-well plates, which were subsequently submitted for transcriptomic analysis using the FLASH-seq method.[30]

Before performing the definitive RNA-seq experiment, we ran a small pilot experiment to optimise FACS strategy before further experiments. In this trial library, neurons represented 89% of cells passing QC with a small cluster of non-neuronal cells expressing *GFAP* evident (Fig. S2d, https://links.lww.com/PAIN/C563). We conducted a principal component analysis using FACS gating

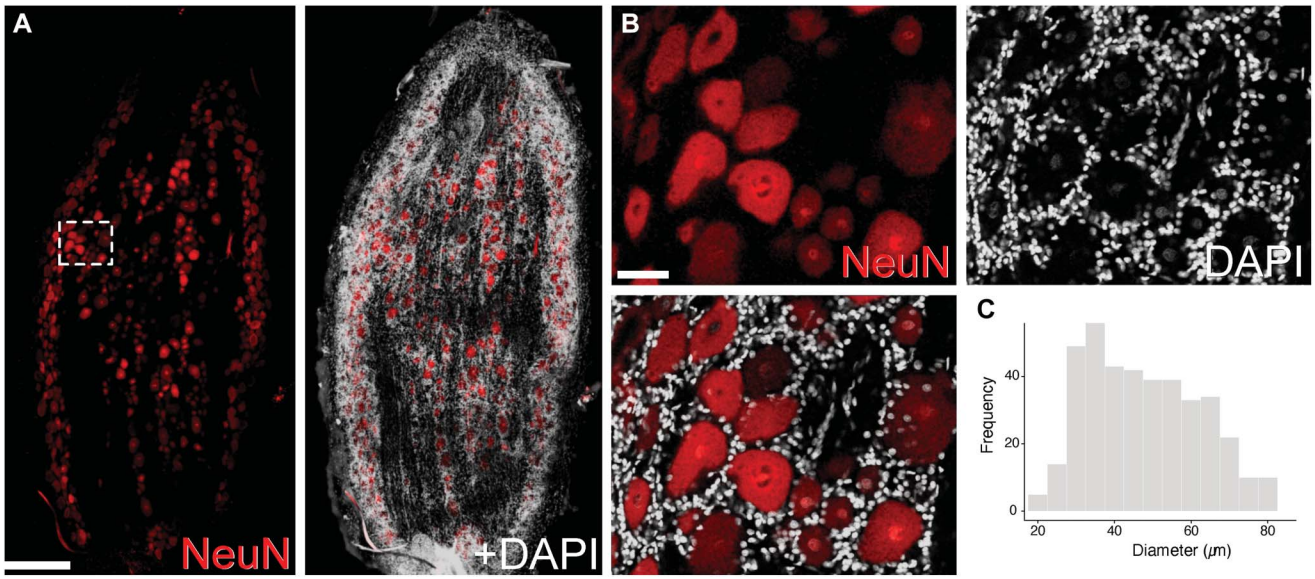


Figure 1. Neuronal size and abundance of non-neuronal cells in the canine DRG. (A) A confocal image of canine DRG stained for NeuN (neurons) and DAPI (all nuclei). (B) Higher magnification views are shown in panels. Large and small neurons are visible surrounded by many non-neuronal cells. Low-resolution image is a maximum projection of 7 optical sections acquired at 2 μm z-resolution, whereas the inset is a single optical section, scale bars are 400 and 50 μm, respectively. (C) Histogram showing the size profile of neurons counted across sections from 4 animals, n = 100 neurons per animal. DRG, dorsal root ganglia.

Copyright © 2026 by the International Association for the Study of Pain. Unauthorized reproduction of this article is prohibited.

parameters to determine if cells in the *GFAP*+ cluster could be excluded by gating. However, *GFAP*+ cells were not distinguishable on this basis (Fig. S2e, https://links.lww.com/PAIN/C563). A moderate number of wells failed to generate data, likely because of plate sorting inaccuracies, resulting in 215 cells passing QC in a 384-well plate. Despite the lower-than-expected yield, these findings demonstrate the feasibility to significantly enrich for neuronal cells before sequencing using this FACS protocol.

3.3. Clusters of canine dorsal root ganglia neurons and marker genes

To generate our final dataset, we sorted an additional 4 plates of cDRG cells and submitted these for sequencing. We used lumbar DRGs from 8 donor beagle dogs of both sexes. Plates were filled over 2 sessions on separate days, using a balanced design where each plate contained cells from a male and female animal. After quality control, and removal of a *GFAP*+ cluster of 93 cells, 934 cells were carried through to the final dataset with a mean unique genes per cell of 8923 (Fig. S3a, https://links.lww.com/PAIN/C563). We examined QC metrics across plate, sex, dog, and session and observed a pattern where cells from female animals were consistently of lower quality (Fig. S3b and c, https://links.lww.com/PAIN/C563), perhaps because of fragmentation of cytoplasm. However, Seurat CCA integration with dog as the batch layer resulted in the same distribution of clusters across sex and plate (Fig. S3d and e, https://links.lww.com/PAIN/C563). To perform CCA, we removed cells from 1 animal (male) from the dataset because of this animal having a number of QC-passing cells (21) that was too low for the integration algorithm, resulting in a final dataset of 913 cells.

Across the clusters, the cells were deemed to be excitatory neurons because of the expression of the neuronal markers *UCHL1* and *TUBB3*, and the glutamate transporter *SLC17A6* (**Fig. 2A**). Genes known to be expressed across broad populations of sensory neurons, such as the Nav1.8 sodium channel (*SCN10A*), the heat-sensitive ion channel *TRPV1*, the μ-opioid receptor (*OPRM1*), the neurotrophin receptors *NTRK1* and *NTRK3*, and the mechanosensitive ion channel *PIEZO2*, were detected across multiple clusters (**Fig. 2B**). We selected a cluster resolution of 1.5, resulting in 12 clusters (d0-d11) to annotate (**Fig. 2C** and Fig. S4, https://links.lww.com/PAIN/C563), we then elected to additionally subdivide the small clusters d5 & d8 because these appeared to include biologically meaningful subtypes of myelinated neurons (**Fig. 2D**). Using known markers for populations of sensory neurons[10,40] (**Fig. 2E** and Fig. S5, https://links.lww.com/PAIN/C563), and unbiased differentially expressed genes (DEGs) (**Fig. 2B**), we annotated the resultant clusters as follows (**Fig. 2F**).

Firstly, a cluster of putative cold sensing neurons (d11) was identified by the expression of the temperature sensing ion channel *TRPM8*, with this cluster also expressing *FOXP2* and *SCN5A*; both established markers of cold-sensitive cells.[10,40] Interestingly, cells in this cluster also expressed high levels of *PENK*, encoding the opioid precursor proenkephalin. We also annotated a cluster (d6) as C-low threshold mechanoreceptors (C-LTMR) on the basis of expression of the marker genes *CDH9*, *TAFA4*, and *P2YR1*.[23] As is the case in humans,[57,85] cells in this cluster did not express the canonical rodent marker genes *SLC17A8* or *TH*.[10]

Two clusters in our dataset resembled non-canonical peptidergic nociceptors. We annotated the first of these (d7) as somatostatin (SST) neurons based on the expression of genes predominantly related to transducing itch-inducing stimuli, including the cytokine receptors *IL31RA* and *OSMR*, the potassium channel *KCNQ4*, and the histamine receptors *HRH1* and *HRH2*.[1,19,82] This cluster was also enriched for *JAK1*, a crucial and targetable component of the downstream effector pathway for cytokine-mediated itch.[12,55] Cells in this cluster also expressed a number of unexpected genes, including *PIEZO1*, *NPYR2*, and the cytokine receptor *IL17RD*. The second cluster (d4) annotated as noncanonical peptidergic expressed classical cross-species markers of noncanonical peptidergic neurons including *MRGPRD*, *GFRA1*, *GFRA2*, and *LPAR3*.[10,40] As has been reported in human DRG,[68,75] these cells also express moderate levels of peptidergic marker genes such as *CALCA* and *TRPV1*, providing evidence that, as seen in other sequencing datasets, a binary division of nociceptors on the basis of peptide expression is not possible in the dog. We also observed selective expression of the ion channel TRPM6 in this population, a channel that is not commonly recognised as a specific feature of sensory neuron clusters in other species.

We identified a number of clusters (d0, d1, d2, d9, and d10) that corresponded to putative unmyelinated C-fibre nociceptors based on the expression of low levels of genes associated with myelination, plus expression of the markers *TRPV1*, *CALCA*, *NTRK1*, *OPRM1*, and *ADCYAP1*.[10,40,78] This set of clusters was annotated on the following basis. The d9 cluster expressed high levels of the *TRPA1* ion channel, akin to a small cluster of C-fibre nociceptors described in humans,[85] and was therefore labelled as C-PEP.TRPA1. Cells within this cluster also expressed low levels of the opioid receptor *OPRK1*, and the serotonin receptor *HTR3A*. Notably, *OPRK1* expression was largely restricted to this cluster, and this pattern of low expression may explain the failure to detect this transcript in previous bulk sequencing studies of cDRG.[35]We labelled the 2 adjacent clusters d1 and d2, based on unbiased marker gene detection (**Fig. 2B**), as C-PEP.GAL and C-PEP.CHRM1. Cells in the C-PEP.GAL cluster expressed galanin and the previously recognised markers of subsets of peptidergic nociceptors *TACR3* and *PROKR2*,[10] whereas cells in the C-PEP.CHRM1 cluster expressed the muscarinic receptor gene *CHRM1*. We named cluster d10 as C-PEP.TRKB because of the expression of the neurotrophin receptor *NTRK2*; however, no single markers linked this cluster to an established class of DRG neuron, and the cross-species analogue of this cluster remains unresolved, although overlap of *CALCA* and *NTRK2* is seen in a single subtype in cross-species atlases (Calca + Dcn in Ref. 10). Finally, we identified a number of cells (cluster d0) that were characterised by a lack of distinctive markers despite the presence of generalised neuronal markers. Previous human DRG datasets, generated using full-length SMART technologies, have also identified similar clusters and termed these hPEP0.[85] We therefore designated this cluster as C-PEP0 in our annotation.

Cluster d3 was characterised by high levels of expression of the proto-oncogene *KIT* and moderate levels of TRPM8 and low levels of TRPV1. A similar cluster of peptidergic nociceptors has recently been described in humans,[85] and we annotated our d3 cluster as PEP-KIT to reflect this apparent similarity. The PEP-KIT cluster also expressed moderate levels of *SLC17A7* and *VSNL1*, which are recognised as cross-species markers of myelinated afferents[40]; however, our gene-expression-based myelination index did not indicate this cluster was heavily myelinated. As such it is currently unclear if this PEP-KIT cluster is myelinated in dogs.

Finally, we annotated the 2 clusters likely containing large, myelinated neurons, as suggested by the myelination index and expression of *NTRK3*. These cells appeared to be underrepresented in our dataset, perhaps because of the FACS sorting protocol biasing towards smaller cells. Using a higher cluster

Copyright © 2026 by the International Association for the Study of Pain. Unauthorized reproduction of this article is prohibited.

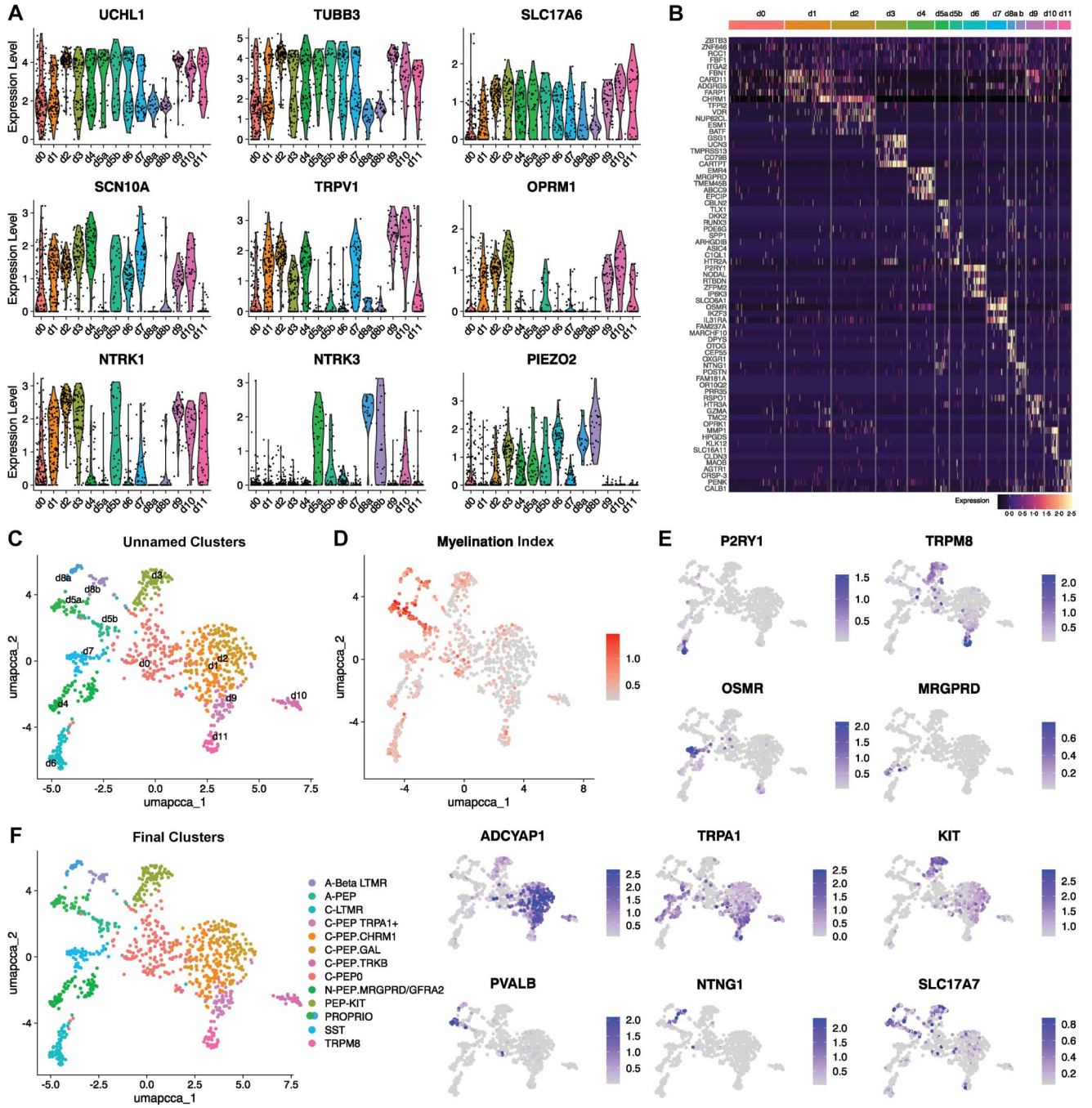


Figure 2. Transcriptomic definition and annotation of canine DRG neuronal subtypes. (A) Violin plots showing expression of broad neuronal markers (*UCHL1*, *TUBB3*, and *SLC17A6*) and core somatosensory genes (*SCN10A*, *TRPV1*, *NTRK1*, *NTRK3*, *OPRM1*, and *PIEZO2*) across all clusters. (B) Heatmap of unbiased differentially expressed genes (DEGs) distinguishing the initial unsupervised clusters. (C) The UMAP projection of FLASH-seq profiles showing clustering of 913 cDRG neurons into transcriptionally distinct groups (d0-d11). (D) Myelination index for each cluster based on an aggregated expression score of myelin-associated genes (*NEFH*, *NEFM*, *SCN8A*, *NFASC*, *KCNQ2*, *KCNQ3*, *KCNA1*, and *CNTN1*), highlighting putative myelinated vs unmyelinated populations. (E) UMAP feature plots illustrating selected cluster-specific marker genes used for manual annotation. (F) Final annotated UMAP showing the resolved sensory neuron subtypes, including C-fibre nociceptors (C-PEP0, C-PEP.TRPA1, C-PEP.GAL, C-PEP.CHRM1, and C-PEP.TRKB), noncanonical peptidergic nociceptors (N-PEP.MRGPRD/GFRA2), SST/OSMR neurons, C-LTMRs, PEP-KIT neurons, proprioceptors, A-δ nociceptors, and A-β LTMRs. cDRG, canine DRG; DRG, dorsal root ganglia; LTMR, low threshold mechanoreceptors.

resolution than could be applied globally, we further subsetted these clusters into clusters d5a, d5b, d8a, and d8b to identify different classes of myelinated afferents. Clusters d5a and d8a were annotated as proprioceptors because of the expression of parvalbumin (*PVALB*). Cluster d5b was identified as a myelinated putative A-delta nociceptor class because of expression of *CALCA* and *SCN10A*. This cluster also expressed the mechanosensitive ion channel *PIEZO2* and the serotonin receptor *HTR2A*. Lastly, the d8b cluster was designated as a group of A-beta LTMRs because of the expression of high levels of *PIEZO2*, the axonal guidance molecule *NTNG1*,[10] and the A-fibre marker *KCNH5*.[85] We also asked if FACS parameters could retrospectively be used to distinguish putative large neurons, as defined by the expression of *NTRK3* (a gene selectively

Copyright © 2026 by the International Association for the Study of Pain. Unauthorized reproduction of this article is prohibited.

expressed in a subset of large neurons), from small neurons, as cell size is known to influence flow parameters. We found no robust FACS parameter-based distinction based on either principal component analysis of all FACS data or pairwise examination of FACS gating measures (Fig. S6, https://links.lww.com/PAIN/C563).

3.4. Cross-species integration reveals convergent and divergent subtype-specific gene expression

Next, we sought to compare cell-type-specific gene expression across species by integrating our canine FLASH-seq cells with existing human and mouse single-cell datasets using 1:1 orthologues. We used Seurat CCA integration to generate cross-species UMAP plots including human cells sequenced using SMARTseq2[85] and an adult mouse dataset with high cell numbers and hence transcriptional coverage.[67] There was significant overlap between clusters (**Fig. 3A**), in particular between the 2 full-length technologies (human and canine). To make cross-species comparisons, we elected to reannotate these cross-species clusters using a simplified unified annotation with 10 clusters (**Figs. 3B and C**). Although the unified cross-species annotation is necessarily coarse, this approach reflects a deliberate trade-off: merging of clusters because of lower cell numbers than droplet-based studies vs exceptionally high molecular depth, thereby permitting robust cross-species comparisons across the annotated clusters.

To determine which molecular features of sensory neurons are shared across species, we first assessed convergent gene expression within each unified cluster. Using a list of physiologically and pharmacologically relevant gene families (ion channels, GPCRs and their ligands, synaptic proteins, transcription factors, and neuropeptides), we identified genes that were robustly detected in both dog and human datasets and were consistently enriched within the same cluster (**Fig. 3D**). This analysis revealed a substantial set of highly conserved markers, many of which represent established therapeutic targets for pain and itch. Notably, transcripts encoding the μ-opioid receptor *OPRM1*, the neurotrophin receptor *NTRK1*, and the nociceptor-enriched sodium channel *SCN10A* showed strong and parallel enrichment across aligned dog–human clusters, indicating the conservation of core nociceptor signalling pathways (**Fig. 3E**). Comparable patterns were also observed when integrating dog and mouse datasets (Table S4, https://links.lww.com/PAIN/C564 & Fig. S7, https://links.lww.com/PAIN/C563). It should be noted that *OPRM1* expression seems comparatively lower in the mouse dataset, consistent with both documented species-level differences in mu-opioid receptor expression in DRG neurons[85] and reduced sensitivity of droplet-based sequencing platforms relative to full-length approaches.

We next examined divergent expression patterns, ie, genes that showed consistent differences between dog and human within the same neuronal cluster. Because artefactual divergence can arise from sparse detection, cluster size differences, or platform-specific dropout, we incorporated minimal detection requirements before testing. Only genes with detectable expression in both species across the datasets were evaluated further. Despite this approach, it is likely that many of the divergent genes likely result from technical factors. However, on examination of the results (Figs. S8 and S9, https://links.lww.com/PAIN/C563), we were able to identify a number of subtype-restricted, species-biased transcripts with relevance to pain and itch. As detailed in subsequent sections, these include *IL31RA*, which in dogs is highly restricted to OSMR/SST neurons, and the somatostatin receptor, *SSTR2*, which shows strikingly broad expression across neuronal subtypes in the dog (Fig. 3f and Fig 3g, https://links.lww.com/PAIN/C563).

3.5. In situ validation of divergent patterns of gene expression relevant to itch and pain therapeutics

We then proceeded to validate the apparent divergent *IL31RA* expression pattern between dogs and humans using in situ hybridisation (ISH). Our cross-species analysis indicated that *IL31RA* is restricted to the SST/OSMR cluster in canine DRG; in contrast to human DRG, where *IL31RA* is additionally expressed in noncanonical peptidergic nociceptors and C-LTMRs (**Fig. 3F**). To verify this, we performed ISH using probes against *IL31RA* alongside *GFRA2*; a conserved marker for C-LTMRs, and noncanonical peptidergic nociceptors in both dogs and humans (Figs S10a and S10b, https://links.lww.com/PAIN/C563). We used canine DRG tissue from 4 animals, of both sexes, and restricted our analysis to neurons expressing *IL31RA* or *GFRA2* (**Fig. 4A**). We counted a mean of 50 (range 36-67) *IL31RA*+ and 180 (115-260) *GFRA2*+ neurons per animal. No neurons co-expressed *IL31RA* and *GFRA2*. To determine if *IL31RA* expression is nonspecific to SST neurons in human DRG, we reanalysed existing, publicly available, human in situ Xenium data.[85] Across 4 Xenium sections, we counted 241 *GFRA2*+ and 266 *IL31RA*+ neurons. Of these, 133 cells co-expressed both genes with 50% of *IL31RA*+ neurons expressing *GFRA2*. (Fig. S10c, https://links.lww.com/PAIN/C563). Overall, these results confirm a restricted *IL31RA* expression pattern in dogs, in striking contrast with human DRG. This species difference has been previously suggested in a canine vs human DRG bulk sequencing dataset,[35] our reanalysis of which shows *IL31RA* transcript abundance to be lower in canine DRG than in humans (Fig. S10d, https://links.lww.com/PAIN/C563). However, here we show that this difference relates to cell-type-specific expression patterns rather than simply differences in absolute expression.

Interestingly, *SSTR2* expression in dogs presents a contrasting pattern to that seen in rodents. In the mouse, *SSTR2* is primarily detected in small-diameter C-fibre nociceptors and is indeed restricted such that it is a canonical subpopulation marker[60]; whereas in dogs, *SSTR2* is seen in small-diameter neuronal populations (C-LTMRs, noncanonical peptidergic nociceptors) but is also highly expressed in PEP-KIT and A-delta nociceptors (small to medium-neuronal diameter). Expression is also seen in some putative A-LTMRs in our dataset. Therefore, we hypothesized that *SSTR2* would be robustly expressed across small- and medium-diameter neurons in cDRG, with expression extending into some medium to large cells. We also hypothesized that a significant proportion of *SSTR2*+ neurons would express high levels of *KIT* and hence would belong to the PEP-KIT population. To investigate this, we again performed ISH in DRGs from 4 donors using *SSTR2* and *KIT* probes (**Fig. 4B**). We first measured the size of all neurons with nuclei present in the sections (n = 1079, Fig. 4c and d, https://links.lww.com/PAIN/C563). Probe signal for *SSTR2* and *KIT* was divided into 3 categories (negative, + and ++; see Methods) and neurons were classified according to their soma diameter into small (<40 μm), medium (40-60 μm), and large (>60 μm). We identified a total of 457 neurons expressing *SSTR2*, of which 254 (58%) co-expressed *KIT* (**Fig. 4E**). Based on diameter, SSTR2 was mostly seen in small to medium neurons although some expression was seen in large neurons (**Fig. 4D**, Table S5, https://links.lww.com/PAIN/C563); whereas, in contrast, *KIT* was primarily a marker of

Copyright © 2026 by the International Association for the Study of Pain. Unauthorized reproduction of this article is prohibited.

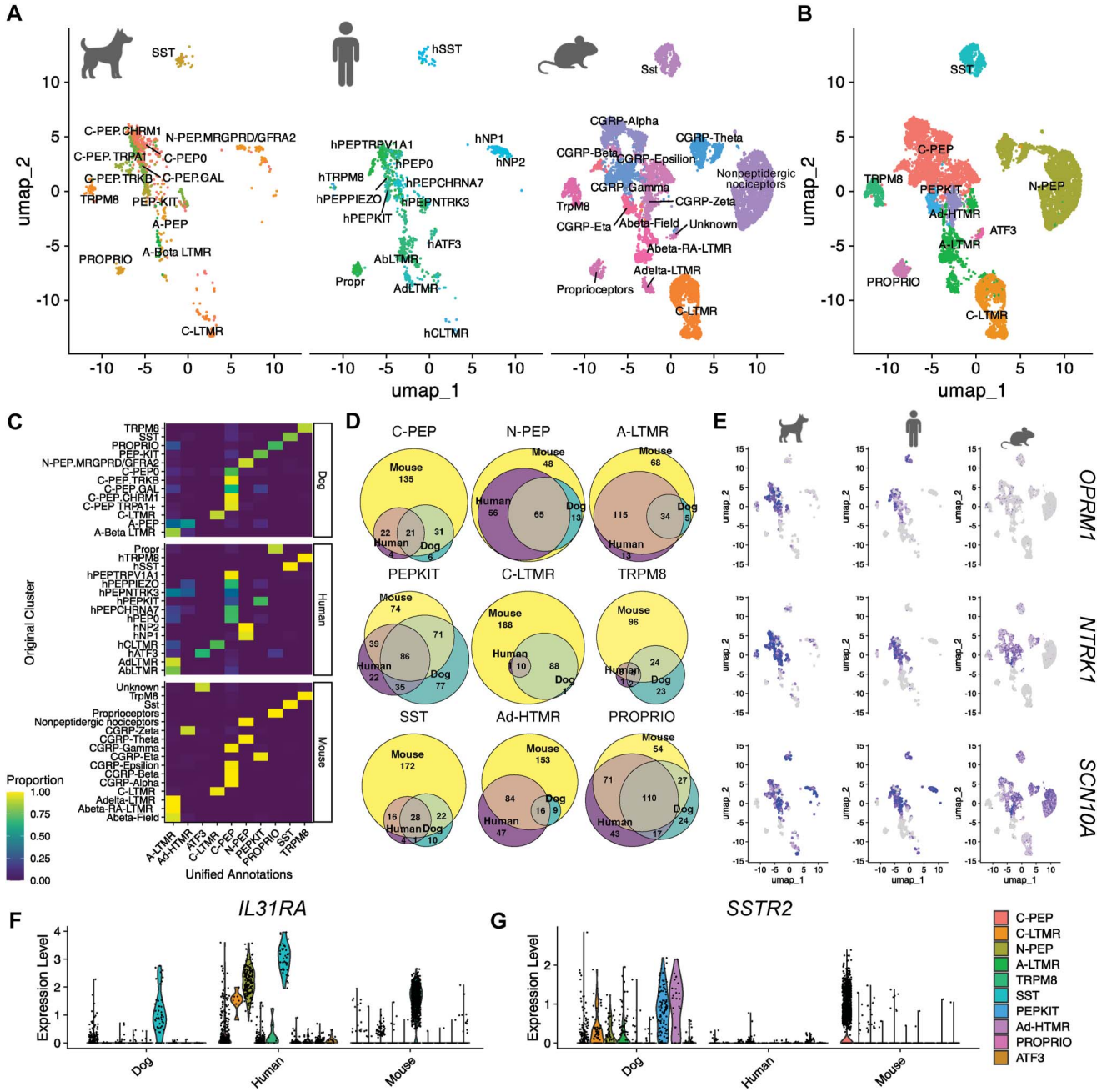


Figure 3. (A) The UMAPs showing integrated dog, human, and mouse DRG datasets coloured by original study-specific cluster identities, illustrating cross-species alignment obtained using 1:1 orthologues and CCA integration. (B) Unified annotation of the integrated dataset collapsed into 10 consensus sensory neuron classes, enabling direct comparison of homologous subtypes across species. (C) Heatmaps showing how original dog, human, and mouse clusters reallocated into the unified consensus annotation after integration. (D) Summary of convergent and divergent DEGs across species within each consensus cluster, highlighting transcripts with conserved enrichment vs species-biased specialisation. (E) Examples of conserved pain- and itch-relevant genes that show strong cross-species alignment in cluster-specific expression patterns. (F–G) Cross-species expression patterns of *SSTR2* and *IL31RA* across neuronal subtypes, illustrating *IL31RA* expression restricted to canine SST/OSMR neurons and the broader *SSTR2* distribution in canine DRG, as quantified in subsequent ISH analyses. CCA, canonical correlation analysis; DEG, differentially expressed gene; DRG, dorsal root ganglia; ISH, in situ hybridisation.

small- to medium-sized neurons (**Fig. 4C**, Table S5, https://links.lww.com/PAIN/C563). Overall, these results show that *SSTR2* expression in dogs is seen in a wider neuronal population than in mice, and this includes cells likely to be nociceptors but also some putative LTMRs based on size profiles.

3.6. Gene expression in canine dorsal root ganglia neurons is likely influenced by domestication

It has been suggested that evolutionary pressures because of domestication have influenced gene expression in other areas of the canine nervous system such as the hippocampus.[89] Dorsal root ganglia sensory neurons arise from the neural crest, an embryonic lineage proposed to be a recurrent target of domestication-related selection,[58] and this raises the possibility that transcriptional specialisation within somatosensory neurons may also carry signatures of domestication. To establish whether this could also be the case, we tested whether putative positively selected genes (PSGs) from published genome-wide domestication scans[4,28,58,80,81] were nonrandomly distributed, ie, enriched, across cDRG transcriptional subtypes. Of all described

Copyright © 2026 by the International Association for the Study of Pain. Unauthorized reproduction of this article is prohibited.

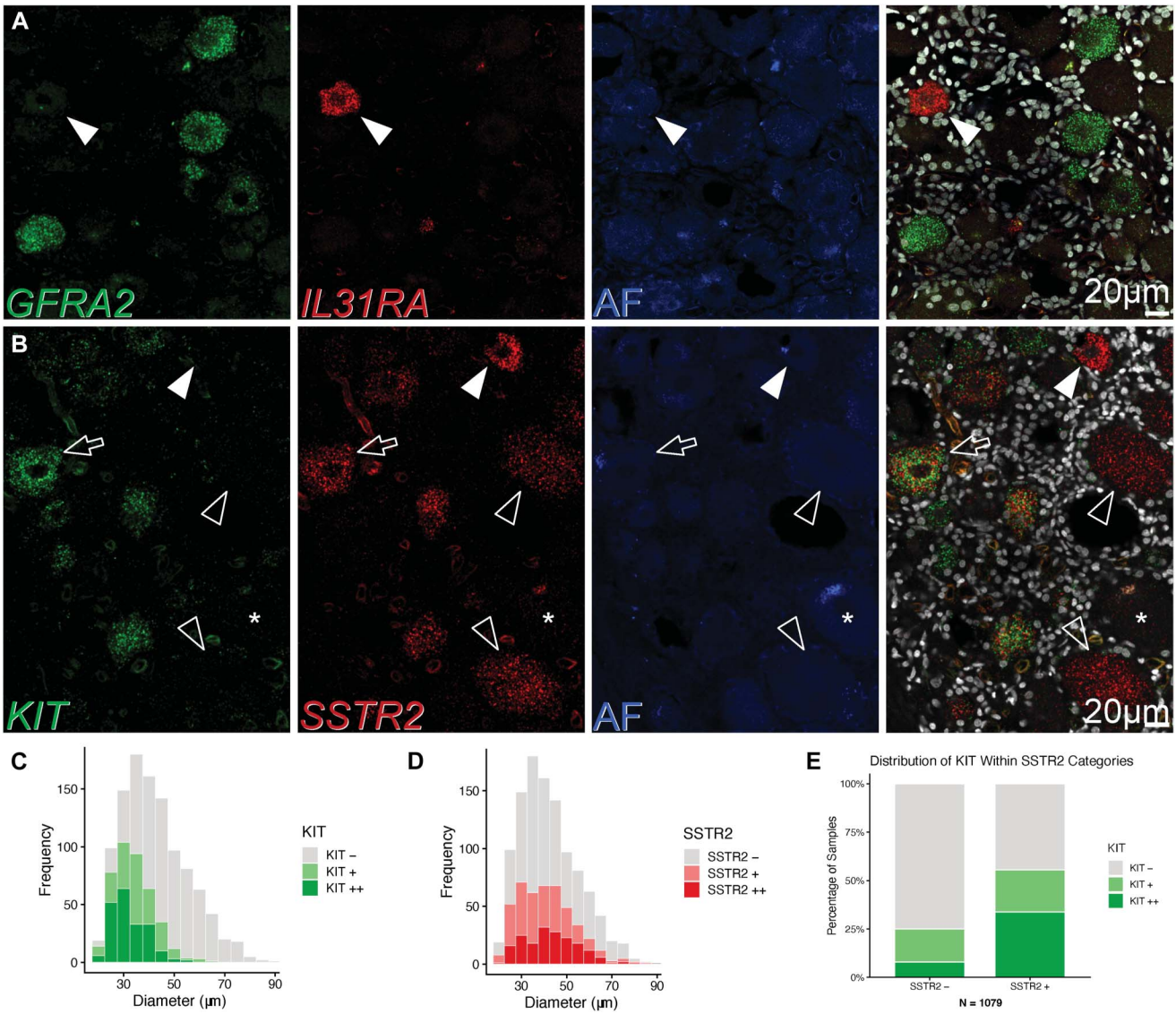


Figure 4. In situ validation of divergent *IL31RA* and *SSTR2* expression patterns in canine DRG. (A) HCR ISH detecting *GFRA2* and *IL31RA* transcripts in canine DRG tissue. The 488-nm channel, acquired in all sections to identify and exclude lipofuscin-associated autofluorescence (AF) from scoring, is shown in blue. Filled arrowhead indicates a single *IL31RA*+ neuron. There is no detectable expression of *IL31RA* in adjacent *GFRA2*+ neurons, confirming the mutually exclusive expression of these markers in dogs. Images represent single confocal optical sections acquired at ×40 magnification. Scale bar = 20 μm. (B) HCR ISH for *KIT* and *SSTR2*. A filled arrowhead indicates a small-diameter neuron expressing *SSTR2*, whereas open arrowheads denote medium-to-large neurons expressing *SSTR2*. The *KIT* expression is seen in subsets of small to medium diameter neurons. Unfilled arrow shows a medium diameter *KIT*+ neuron with high *SSTR2* expression. A large-diameter neuron lacking *SSTR2* expression is marked by a star. Images are single confocal optical sections acquired at ×40 magnification. Scale bar = 20 μm. (C) Soma-diameter distribution of KIT^+ neurons, demonstrating that *KIT* expression spans small- and medium-sized neuronal populations. (D) Soma-diameter distribution of *SSTR2*+ neurons illustrating expansion of expression beyond the small-diameter range into medium-sized neurons. (E) Quantification of *KIT* expression within $SSTR2^+$ and $SSTR2^-$ neurons. DRG, dorsal root ganglia; ISH, in situ hybridisation.

PSGs, 573 were detectably expressed and were included in enrichment analyses.

Hypergeometric analysis revealed significant overrepresentation of PSGs in a subset of DRG neuronal clusters (**Table 1**). A separate 1000-permutation analysis confirmed the same set of nonrandom enrichments of PSGs in clusters. The strongest enrichments were observed in peptidergic C fibres, noncanonical peptidergic C fibres, C-LTMRs, proprioceptors, and SST neurons. The convergence of both statistical approaches supports a biologically meaningful overrepresentation of domestication-associated genes within specific DRG neuronal lineages and may demonstrate that canine domestication has preferentially impacted specific sensory neuron pathways.

Furthermore, we selected example genes with roles in pain and itch (**Table 1**) from the full lists of enriched PSGs (Table S6, https://links.lww.com/PAIN/C563) to demonstrate that many potentially selected genes are linked to neuronal signalling and sensory function. Of note, *IL31RA* has been previously documented as being influenced by domestication and its enrichment within specific cDRG neuronal subtypes suggests that evolutionary pressures may have influenced the regulatory context of *IL31RA* in dogs.[58] Overall, the over-representation of PSGs in cDRG transcriptional clusters suggests that selection associated with domestication may have systematically shaped pain, itch, and mechanosensory circuits in the dog, thereby generating species-specific transcriptional programs for sensory function.

Copyright © 2026 by the International Association for the Study of Pain. Unauthorized reproduction of this article is prohibited.

3.7. Canine atlas generation and label transfer from a large human dataset confirms cluster identities

Finally, we validated our single-cell clusters by integrating them with an independently generated single-nucleus canine DRG dataset produced by a collaborating group.[39]This cross-platform integration combined our deep, full-length FLASH-seq profiles with a large-scale 10× Chromium snRNA-seq dataset. This substantially increased total cell numbers and expanded transcriptional coverage while preserving the high-resolution molecular detail that distinguishes our dataset. The 2 canine datasets showed strong concordance, with clear alignment of major sensory neuron classes, robust cross-platform reproducibility of cluster identities, and improved representation of large-diameter neuronal populations that were relatively undercaptured by FACS (**Fig. 5A**). Together, these analyses enabled consensus cluster naming, finer-grained annotation of neuronal subtypes, and the construction of a unified canine DRG atlas that will serve as a valuable comparative resource for future sensory neurobiology. Full details of the atlas generation and benchmarking are provided in the companion paper.[39]

In addition to the cross-platform canine integration, we further benchmarked our clusters against human sensory neuron diversity by performing Seurat label transfer from a recently generated multistudy human consensus atlas from the NIH PRECISION human pain network,[11] which defines 22 neuronal classes. This analysis provided an independent, cross-species validation of our annotations and allowed us to identify the closest human counterparts for each cDRG subtype. Although some canine clusters—particularly within the C-nociceptor and proprioceptor groups—mapped onto multiple human subpopulations, the key neuronal types central to our ISH analyses (C-LTMR, PEP-KIT, SST/OSMR, and nonpeptidergic nociceptors) showed strong and unambiguous alignment with their human equivalents (**Fig. 5B**). This convergence across datasets supports the conclusion that the cross-species comparisons underpinning our *IL31RA* and *SSTR2* analyses rest on a conserved framework of sensory neuron identities.

4. Discussion

Our study provides a deeply sequenced single-cell atlas of purified canine DRG neurons, generated using flash-frozen postmortem tissue by a novel FACS-based enrichment strategy combined with FLASH-seq. This dataset reveals the organisation of canine sensory neuron subtypes and establishes points of both similarity and divergence with human and mouse DRG.

4.1. Sorting-based enrichment of neurons for FLASH-seq

Neuronal isolation from the DRG is challenging because of the predominance of non-neuronal cells. The neuron to non-neuronal cell ratio in cDRG is similar to human,[88] but significantly lower than in rodents.[3] In human DRG, laser-capture has been used to isolate individual neuronal somata.[85] To address this, we developed a FACS-based workflow that enriches for intact canine DRG neurons and preserves soma integrity. Although current FACS parameters do not achieve clear size-based discrimination of large vs small neurons, our dissociation method maintains the full soma, unlike single-nucleus workflows. By measuring cell size with emerging imaging-enabled cell sorters,[46] it may soon be possible to selectively enrich LTMR- vs nociceptor-sized neurons directly from flash-frozen postmortem tissue. Such an approach could support targeted bulk-sequencing of DRG neurons from animals or human patients with defined painful conditions.

This is the first application of FLASH-seq to canine DRG neurons. Despite the modest number of sorted cells, the resulting dataset exhibits high-quality transcriptomes, characterised by high unique gene detection and minimal mitochondrial content. Plate-based sequencing inherently captures fewer cells than droplet-based methods, and is therefore less effective for detection of rare cell clusters, but provides much greater transcriptional depth alongside transcript-level information that could in principle be interrogated in future.[30,41] In our dataset, neurons generally exhibited a high number of detected genes, and this resulted in well-resolved clusters, even with fewer than 1000 cells sequenced. Nonetheless, some clusters were under-represented, particularly those corresponding to large-diameter

Table 1

Enrichment of positively selected genes across canine dorsal root ganglia neuronal subtypes.

Cluster	PSG overlap (n)	Hypergeometric *P* adjusted	Permutation *P*	Selected PSGs (exemplars)
C-PEP.GAL	207	1.06e-07	<1.00e-03	OPRM1, GNAQ, NGFR, TLX3, GPR139
C-PEP.TRPA1	136	1.35e-05	<1.00e-03	OPRM1, FOXP2, GPR139, COL11A1, CACNB3
N-PEP.MRGPRD/GFRA2	50	3.13e-03	1.00e-03	CISH, PLCE1, KCNC2, GRB10, GPR139
C-LTMR	50	3.23e-03	<1.00e-03	GAD2, FGF1, GRB10, CISH, CNTN5
PROPRIO	70	3.23e-03	3.00e-03	CALB2, NTNG1, CNTN5, FGF1, MAPKAPK3
SST	35	6.37e-03	1.00e-03	IL31RA, GPR139, PLCE1, CYP1B1, TIAM1
C-PEP.TRKB	61	1.22e-02	7.00e-03	OPRM1, NGFR, GAD2, TCF4, GNAQ
C-PEP.CHRM1	24	4.28e-01	2.84e-01	GPR139, SCN2A, COL11A1, NRXN3
A-PEP	9	4.47e-01	3.54e-01	NGFR, SEMA3D, GALR1, ADCY8
C-PEP0	36	4.47e-01	3.07e-01	IKZF1, C5AR1, PITX1
PEP-KIT	100	4.47e-01	3.56e-01	OPRM1, NRXN3, CACNA1A, LRRTM3
TRPM8	12	7.75e-01	6.96e-01	FOXP2, CALB2, NKAIN2
A-Beta LTMR	160	7.75e-01	7.76e-01	NTNG1, GALR2, CNTN5, CACNA1A, ADM

For each transcriptional cluster, the number of PSGs overlapping the cluster-specific DEG set is shown together with enrichment significance assessed by hypergeometric testing (BH-adjusted across 13 clusters) and by 1000 permutation testing (values of 0/1000 reported as <1.00e-03). Selected PSGs list representative domestication-associated genes present in each cluster's PSG vs DEG set.
DEG, differentially expressed gene; LTMR, low threshold mechanoreceptors; PSG, positively selected gene.

Copyright © 2026 by the International Association for the Study of Pain. Unauthorized reproduction of this article is prohibited.

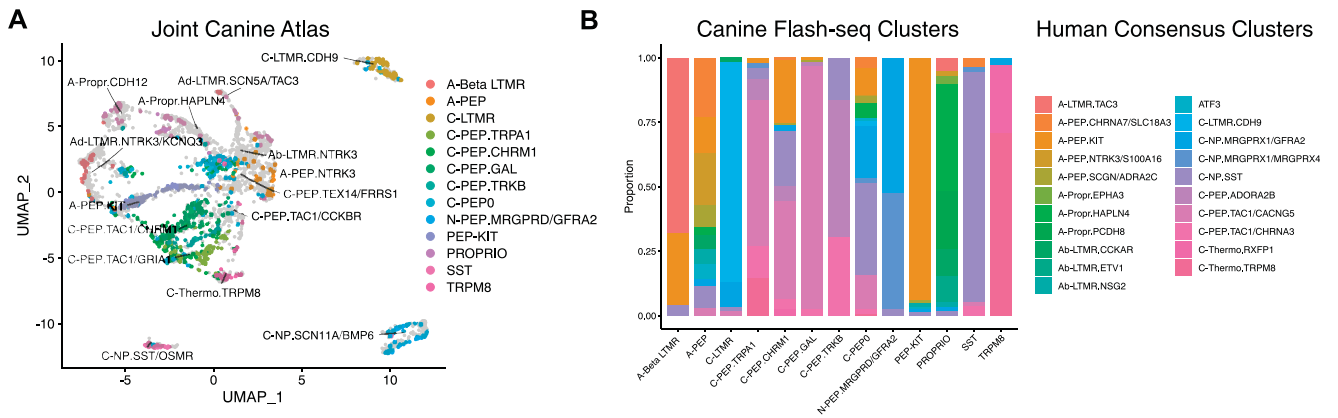


Figure 5. Cross-platform canine atlas and cross-species label transfer to human DRG. (A) Joint canine DRG atlas generated by integrating the deep full-length FLASH-seq dataset with an independently produced 10× chromium single-nucleus DRG dataset. Colours indicate cluster identity according to the FLASH-seq annotations in this article. Gray points represent cells from the independent 10× dataset. Names on the UMAP plot itself represent the consensus cluster names from the canine atlas. (B) Stacked bar plot showing results of cross-species label transfer from the NIH PRECISION human DRG consensus atlas, mapping FLASH-seq cell classes onto newly described human sensory neuron clusters. DRG, dorsal root ganglia.

neurons such as LTMRs and proprioceptors. Although we successfully detected these populations, they were likely biased against during FACS because of technical considerations.

We also observed a lower number of unique genes detected in tissue from female vs male dogs. We interpret these differences as potentially reflecting sex-dependent variation in membrane robustness or intracellular matrix properties ultimately affecting cell integrity during dissociation. Because sequencing depth varied between sexes, the present dataset cannot be used to draw meaningful biological conclusions about sex-dependent gene expression, despite this being an area of considerable interest in sensory neuroscience.[27,29,53,70] Nonetheless, clustering remained relatively stable between male and female-derived neurons, indicating that the overall transcriptional architecture is preserved despite these technical effects.

4.2. A broadly conserved sensory neuron architecture across species

In our dataset, we identify cardinal classes of sensory neuron that are, perhaps unsurprisingly, similar to those described across mammals.[10,40]Given the translational value of the dog, we were particularly interested in whether the canine DRG might be more like human rather than rodent ganglia. We first identified a proportion of non-neuronal cells in cDRG akin to that seen in humans. Given the growing literature surrounding the importance of neuroimmune interactions in pain,[20,33,38,71] this comparative similarity in cellularity is a potential benefit when using the dog for translation. We did not establish similarity at the level of specific immune cell populations, but others have recently found important commonalities between canine and human microglia-like cells, which are not mirrored in rodent DRG tissue.[84]

Our results also point to an overall organisation of peptidergic nociceptors that is unlike that seen in rodents. Murine studies reveal clear separation among peptidergic nociceptor subtypes. Although terminology varies, these subtypes are commonly termed PEP 1.1/1.2/1.3/1.4, CGRP-Alpha/Beta/Gamma/Epsilon or CGRP + Sstr2/Dcn/Adra2a/Oprk1.[10,45,67] In humans, these classes are less distinct and conflated into 2 classes.[85] Both our clustering and cross-species UMAPs show that canine peptidergic clusters are also less distinct according to the resolution afforded by our cell numbers. Beyond the peptidergic nociceptors, several canine marker genes resemble human rather than rodent patterns. *CALCA* is more widely expressed across nociceptive populations in cDRG (see Fig. S5, https://links.lww.com/PAIN/C563), in particular in SST-expressing cells, as has also been shown in humans.[68,69,85] We also see limited canine expression of some classical marker genes, eg, *TH* and *SLC17A8* in C-LTMRs, with human marker genes such as CDH9 more highly expressed.[11] Furthermore, we identify a specific cluster of neurons, termed PEP0, identified previously only in human deep sequencing data.[85] PEP0 neurons have been suggested as a human specific population of A-fibre nociceptors, identified in both sequencing and Xenium spatial data,[85] that express moderate levels of *CALCA* and *PIEZO2* but do not have a clear function. In our data, we see a similar population of neurons that meet QC thresholds but lack specific marker genes. Although these cells could simply represent low-quality neurons, we believe this to be unlikely because of the low percentage of mitochondrial reads and the observation that the cluster is still present when significantly higher QC thresholds are used. To date, PEP0 type cells have only been identified in deep, plate-based sequencing datasets, and it is possible that their detection is biased against by more commonly used microfluidic sequencing methodologies.

Our data also integrates well with other sequencing datasets, further validating our clustering and highlighting more clearly the biological organisation of canine sensory populations. Combining our deeply sequenced dataset with another recent 10×-generated dataset[39] shows that canine cell types are generally analogous across technologies within species and results in a collaborative resource with higher transcriptional coverage than each single study. Our data also aligns well across species to humans, with both single datasets[85] and consensus atlases[11] showing good agreement. This agreement is strongest in the case of the PEP-KIT neurons, noncanonical peptidergic nociceptors, SST/OSMR neurons, and C-LTMRs, which were the focus of our cross-species in situ experiments

4.3. Rational cross-species therapeutic target identification

Our target-focused, cross-species comparison shows how gene expression differs in DRG neuron subtypes across species and hence how this may affect translation of therapeutics. This

Copyright © 2026 by the International Association for the Study of Pain. Unauthorized reproduction of this article is prohibited.

analysis identified a set of highly conserved genes across dog, human, and mouse DRG, including *OPRM1*, *NTRK1*, and *SCN10A*. These targets show conserved, subtype-specific enrichment across all 3 species, supporting the view that these core nociceptor signalling molecules are likely to be pharmacologically tractable across dogs, humans, and rodents. Consistent with this, each of these 3 genes is already the basis of successful analgesic therapies in clinical or veterinary clinical use.[25,64,79]

However, divergence in the expression of other potentially therapeutically relevant genes highlights important species-specific specialisations. We focused on 2 examples, *IL31RA* and *SSTR2*, where cross-species differences may have direct implications for both drug mechanisms and genetic access strategies.

In the case of *IL31RA*, we observed a strikingly restricted neuronal expression pattern in the dog, where *IL31RA* expression is confined to the SST/OSMR population. By contrast, human DRG shows a distributed pattern where *IL31RA* is expressed across noncanonical peptidergic nociceptors and CLTMRs in addition to SST neurons. This was confirmed through in situ hybridisation in both species. These neuronal subtypes possess distinct spinal projections and engage different downstream circuits.[22,54,60,77] Therefore, this divergence suggests that IL31-targeted therapies may modulate a qualitatively different itch percept in dogs and humans. Extending beyond circuitry, *IL31RA* has previously been identified as a domestication associated gene,[58] and its reduced abundance in dogs raises the possibility, albeit speculative, that selection pressures related to a desire to increase parasite tolerance during cohabitation may have shaped IL31-dependent itch pathways. This theory is consistent with the finding that dogs do not scratch consistently in response to many common experimental pruritogens.[6,18] Interestingly, *IL31RA* agonism has recently been reported to act as an immunological brake, reducing the severity of skin inflammation in pruritic conditions.[26] It is therefore possible that comparatively reduced *IL31RA* expression could also be a factor underlying high prevalence of atopic dermatitis in dogs.[24]

In the dog, we find *SSTR2* to be expressed across a broad set of sensory neuron subtypes, spanning small-diameter nociceptors through to medium diameter neurons and even some LTMR-like cells. This contrasts with the situation in rodents, where *SSTR2* marks a discrete nociceptor subclass recently implicated in spontaneous neuropathic pain[87]; making those cells appealing for targeted therapies. Importantly, this divergence likely reflects changes in marker gene identity, not the absence of the underlying cell class, but nonetheless has substantial implications for gene targeting approaches that require molecularly specific access points.[45,50] Whether the human *SSTR2* pattern more closely resembles dog or mouse remains unresolved, although it seems that *SSTR4* is a more appealing analgesic target in humans with the potential for fewer endocrine side effects.[14,74] Interestingly, *SSTR4* has not yet been identified in the canine genome, and this underscores the need for continued comparative profiling.[37] Together, these examples illustrate that while many key sensory targets are conserved, species-specific transcriptional features may affect both the mechanisms and the translational relevance of pain and itch therapies.

In conclusion, our results establish a high-resolution resource and demonstrate that deep, full-length profiling of purified cells from frozen post-mortem tissue is feasible. Using these data, we outline the conserved and divergent, and in places potentially domestication shaped, sensory pathways that refine the dog's translational value for pain and itch.

Conflict of interest statement

The authors have no conflict of interest to declare.

Acknowledgements

The work was supported by a PhD studentship grant from the University of Glasgow Vet Fund. A.M.B. is supported by a Wellcome Trust Early-Career Award (304005/Z/23/Z), and G.A.W. is supported by an MRC grant UKRI3822.

The authors are grateful to the Scottish SPCA and Charles River Laboratories for their kind assistance with sourcing canine tissues for this project. The authors acknowledge the expert assistance of Daniel Lewis and Diane Vaughan, MVLS-SRF Flow Cytometry Core Lab at the University of Glasgow. The authors are grateful to Andrew McCluskey and Joy Kabagenyi for their guidance in analysis of the single-cell dataset and to Matthew Sapio and Michael Iadarola for their assistance with reanalysis of their existing bulk sequencing data. The authors also thank Leanne Jankelunas, Shamsuddin Bhuiyan, William Renthal, and Rell Parker for their collaborative role in generating the canine 10× atlas and for their continued engagement, discussion and assistance during the preparation, and submission of this and the companion manuscript.

Raw sequencing data and processed files including the Seurat object are available at the Gene Expression Omnibus (GSE327952). An interactive browser of FLASH-seq data is available at https://canineflashseq.shinyapps.io/Browser/. All other data and analysis files are freely available at the University of Glasgow's Enlighten repository (https://doi.org/10.5525/gla.researchdata.2399).

For the purpose of open access, the author has applied a Creative Commons Attribution (CC-BY) licence to any Author Accepted Manuscript version arising from this submission.

Supplemental digital content

Supplemental digital content associated with this article can be found online at https://links.lww.com/PAIN/C563, https://links.lww.com/PAIN/C564.

Article history:
Received 14 April 2026
Received in revised form 9 June 2026
Accepted 12 June 2026
Available online 2 September 2026

References

[1] Akiyama T, Carstens E. Neural processing of itch. Neuroscience 2013; 250:697–714.
[2] Arnold C. Sick as a dog: how understanding canine diseases will save human lives. Nat Med 2022;28:1970–3.
[3] Avraham O, Feng R, Ewan EE, Rustenhoven J, Zhao G, Cavalli V. Profiling sensory neuron microenvironment after peripheral and central axon injury reveals key pathways for neural repair. Elife 2021;10:e68457.
[4] Axelsson E, Ratnakumar A, Arendt M-L, Maqbool K, Webster MT, Perloski M, Liberg O, Arnemo JM, Hedhammar A, Lindblad-Toh K. The genomic signature of dog domestication reveals adaptation to a starch-rich diet. Nature 2013;495:360–4.
[5] Bankhead P, Loughrey MB, Fernández JA, Dombrowski Y, McArt DG, Dunne PD, McQuaid S, Gray RT, Murray LJ, Coleman HG, James JA, Salto-Tellez M, Hamilton PW. QuPath: open source software for digital pathology image analysis. Sci Rep 2017;7:16878.
[6] Banovic F, Denley T, Blubaugh A. Dose-dependent pruritogenic and inflammatory effects of intradermal injections of histamine, compound 48/80 and anti-canine IgE in healthy dogs. Vet Dermatol 2019;30:325.

Copyright © 2026 by the International Association for the Study of Pain. Unauthorized reproduction of this article is prohibited.

[7] Basbaum AI, Bautista DM, Scherrer G, Julius D. Cellular and molecular mechanisms of pain. Cell 2009;139:267–84.
[8] Bates MC, Roady P, Lehner AF, Buchweitz JP, Heggem-Perry B, Lezmi S. Atypical bromethalin intoxication in a dog: pathologic features and identification of an isomeric breakdown product. BMC Vet Res 2015;11:244.
[9] Berta T, Strong JA, Zhang J-M, Ji R-R. Targeting dorsal root ganglia and primary sensory neurons for the treatment of chronic pain: an update. Expert Opin Ther Targets 2023;27:665–78.
[10] Bhuiyan SA, Xu M, Yang L, Semizoglou E, Bhatia P, Pantaleo KI, Tochitsky I, Jain A, Erdogan B, Blair S, Cat V, Mwirigi JM, Sankaranarayanan I, Tavares-Ferreira D, Green U, McIlvried LA, Copits BA, Bertels Z, Del Rosario JS, Widman AJ, Slivicki RA, Yi J, Sharif-Naeini R, Woolf CJ, Lennerz JK, Whited JL, Price TJ, Gereau Iv RM, Renthal W. Harmonized cross-species cell atlases of trigeminal and dorsal root ganglia. Sci Adv 2024;10:eadj9173.
[11] Bhuiyan SA, Nagi SS, Sankaranarayanan I, Semizoglou E, Usoskin D, Yang L, Yu H, Arendt-Tranholm A, Bertels Z, Bhatia P, Bouchatta O, Boyer K, Cervantes A, Chalif J, Chintalapudi H, Cicalo A, Copits B, Cronin C, Curatolo M, Dong X, Dougherty PM, Dourson A, Funk G, Gabriel K, Griesemer DS, Guo H, Gupta P, Hofstetter C, Horton P, Hsieh A, Inturi NN, Jain A, Jayakar S, Johnston B, Kim R, Krauter D, Kupari J, Lemen J, Lesnak JB, Liu W, Lopez I, Lu Y, MacMillan HJ, Mazhar K, Meriau P, Moffitt JR, Moreno MM, Mwirigi JM, Naz H, O'Brein J, Payne M, Del Rosario J, Rosen SF, Shiers S, Simpson E, Slivicki R, Stone JR, Tavares-Ferreira D, Uhelski M, Woolf CJ, Xu Q, Yi J, Yousuf MS, Zhu D, Cavalli V, Zhao G, Olausson H, Ernfors P, Gereau RW, Luo W, Price TJ, Renthal W. NIH PRECISION human pain network. A reference Atlas of the human dorsal root ganglion. bioRxiv. 2025. https://doi.org/10.1101/2025.11.05.686654.
[12] Bieber T, Simpson EL, Silverberg JI, Thaçi D, Paul C, Pink AE, Kataoka Y, Chu C-Y, DiBonaventura M, Rojo R, Antinew J, Ionita I, Sinclair R, Forman S, Zdybski J, Biswas P, Malhotra B, Zhang F, Valdez H. Abrocitinib versus placebo or dupilumab for atopic dermatitis. N Engl J Med 2021;384:1101–12.
[13] Bimonte S, Cascella M, Forte CA, Esposito G, Cuomo A. The role of anti-nerve growth factor monoclonal antibodies in the control of chronic cancer and non-cancer pain. J Pain Res 2021;14:1959–67.
[14] Bjørn-Yoshimoto WE, Ramiro IBL, Koch TL, Engholm E, Yeung HY, Sørensen KK, Goddard CM, Jensen KL, Smith NA, Martin LF, Smith BJ, Madsen KL, Jensen KJ, Patwardhan A, Safavi-Hemami H. Cone snail venom-inspired somatostatin receptor 4 (SSTR4) agonists as new drug leads for peripheral pain. Sci Rep 2025;15:42638.
[15] BPS guide to pharmacology. Available at: https://www.guidetopharmacology.org/targets.jsp. Accessed March 31, 2026.
[16] Braz J, Solorzano C, Wang X, Basbaum AI. Transmitting pain and itch messages: a contemporary view of the spinal cord circuits that generate gate control. Neuron 2014;82:522–36.
[17] Brown DC, Coetzee J, Gill M, Johnson C, Mohapatra DP, Oshinsky ML, Robertson SA, Smith ER, Lascelles BDX. Outcome assessment in veterinary pain studies: a pain in animals workshop (PAW) perspective. Front Pain Res (Lausanne) 2025;6:1579155.
[18] Carr MN, Torres SMF, Koch SN, Reiter LV. Investigation of the pruritogenic effects of histamine, serotonin, tryptase, substance P and interleukin-2 in healthy dogs. Vet Dermatol 2009;20:105–10.
[19] Cevikbas F, Wang X, Akiyama T, Kempkes C, Savinko T, Antal A, Kukova G, Buhl T, Ikoma A, Buddenkotte J, Soumelis V, Feld M, Alenius H, Dillon SR, Carstens E, Homey B, Basbaum A, Steinhoff M. A sensory neuron-expressed IL-31 receptor mediates T helper cell-dependent itch: involvement of TRPV1 and TRPA1. J Allergy Clin Immunol. 2014;133:448–60.e7. https://doi.org/10.1093/brain/awag088.
[20] Chrysostomidou P, Hore Z, Somma D, Vlachaki Walker JM, Diallo K, Titterton HF, Elmesmari A, Schino L, Adesida S, Kurowska-Stolarska M, Denk F, Weir GA. Macrophages amplify spontaneous activity of damaged sensory neurons in a human co-culture model of neuropathic pain. Brain. 2026. https://doi.org/10.1093/brain/awag088.
[21] Clark JD. Preclinical pain research: can we do better? Anesthesiology 2016;125:846–9.
[22] Davis OC, Dickie AC, Mustapa MB, Boyle KA, Browne TJ, Gradwell MA, Smith KM, Polgár E, Bell AM, Kókai É, Watanabe M, Wildner H, Zeilhofer HU, Ginty DD, Callister RJ, Graham BA, Todd AJ, Hughes DI. Calretinin-expressing islet cells are a source of pre- and post-synaptic inhibition of non-peptidergic nociceptor input to the mouse spinal cord. Sci Rep 2023;13:11561.
[23] Delfini M-C, Mantilleri A, Gaillard S, Hao J, Reynders A, Malapert P, Alonso S, François A, Barrere C, Seal R, Landry M, Eschallier A, Alloui A, Bourinet E, Delmas P, Le Feuvre Y, Moqrich A. TAFA4, a chemokine-like protein, modulates injury-induced mechanical and chemical pain hypersensitivity in mice. Cell Rep 2013;5:378–88.
[24] Drechsler Y, Dong C, Clark DE, Kaur G. Canine atopic dermatitis: prevalence, impact, and management strategies. Vet Med Res Rep 2024;15:15–29.
[25] Enomoto M, Mantyh PW, Murrell J, Innes JF, Lascelles BDX. Anti-nerve growth factor monoclonal antibodies for the control of pain in dogs and cats. Vet Rec 2019;184:23.
[26] Fassett MS, Braz JM, Castellanos CA, Salvatierra JJ, Sadeghi M, Yu X, Schroeder AW, Caston J, Munoz-Sandoval P, Roy S, Lazarevsky S, Mar DJ, Zhou CJ, Shin J-S, Basbaum AI, Ansel KM. IL-31–dependent neurogenic inflammation restrains cutaneous type 2 immune response in allergic dermatitis. Sci Immunol 2023;8:eabi6887.
[27] Finn DP, McGuire BE, Beggs S, Boerner KE, Davis KD, Defrin R, De Koninck Y, Devan H, Donovan R, Fetter E, Flor H, Fullen BM, Healy CR, Keogh E, Kuner R, Kunz M, Lane RM, Lautenbacher S, Mayer EA, Mogil JS, O'Mahony SM, O'Sullivan K, Riordan L, Salter MW, Scarlatti F, Shorten G, Sluka KA, Stinson JN, Vowles KE, Walker SM, Yalcin I, Roche M. Recommendations for the inclusion and study of sex and gender in research. Nat Neurosci 2026;29:256–66.
[28] Freedman AH, Schweizer RM, Ortega-Del Vecchyo D, Han E, Davis BW, Gronau I, Silva PM, Galaverni M, Fan Z, Marx P, Lorente-Galdos B, Ramirez O, Hormozdiari F, Alkan C, Vilà C, Squire K, Geffen E, Kusak J, Boyko AR, Parker HG, Lee C, Tadigotla V, Siepel A, Bustamante CD, Harkins TT, Nelson SF, Marques-Bonet T, Ostrander EA, Wayne RK, Novembre J. Demographically-based evaluation of genomic regions under selection in domestic dogs. PLoS Genet 2016;12:e1005851.
[29] Gambeta E, Salter MW. Microglia, sex, and pain: even more twists and turns ahead? PAIN 2025;166:S23–6.
[30] Hahaut V, Pavlinic D, Carbone W, Schuierer S, Balmer P, Quinodoz M, Renner M, Roma G, Cowan CS, Picelli S. Fast and highly sensitive full-length single-cell RNA sequencing using FLASH-seq. Nat Biotechnol 2022;40:1447–51.
[31] HGNC download files overview. HUGO Gene Nomenclature Committee. Available at: https://www.genenames.org/download/. Accessed March 31, 2026.
[32] Hockley JRF, Taylor TS, Callejo G, Wilbrey AL, Gutteridge A, Bach K, Winchester WJ, Bulmer DC, McMurray G, Smith ESJ. Single-cell RNAseq reveals seven classes of colonic sensory neuron. Gut 2019;68:633–44.
[33] Hodges PW, Fiore NT, Watkins LR, Klyne DM, Coppieters MW, Grace PM. Pain and the immune system. Musculoskelet Sci Pract 2026;82:103484.
[34] Hunt J, Knazovicky D, Lascelles BDX, Murrell J. Quantitative sensory testing in dogs with painful disease: a window to pain mechanisms? Vet J 2019;243:33–41.
[35] Iadarola MJ, Sapio MR, Raithel SJ, Mannes AJ, Brown DC. Long-term pain relief in canine osteoarthritis by a single intra-articular injection of resiniferatoxin, a potent TRPV1 agonist. PAIN 2018;159:2105–14.
[36] Iadarola MJ, Brown DC, Nahama A, Sapio MR, Mannes AJ. Pain treatment in the companion canine model to validate rodent results and incentivize the transition to human clinical trials. Front Pharmacol 2021;12:705743.
[37] Immler M, Wolfram M, Oevermann A, Walter I, Wolfesberger B, Tichy A, Gradner G. Expression of somatostatin receptors in canine and feline meningioma. Vet Med Sci 2024;10:e1537.
[38] Jain A, Hakim S, Woolf CJ. Immune drivers of physiological and pathological pain. J Exp Med 2024;221:e20221687.
[39] Jankelunas L, Bhuiyan SA, Macmillan HJ, Cecere T, Bertke A, Rossmeisl JH, Renthal W, Parker RL. Translational insights into canine dorsal root ganglia cell types using cross-species comparisons. bioRxiv. 2026. https://doi.org/10.64898/2026.04.14.718477.
[40] Jung M, Dourado M, Maksymetz J, Jacobson A, Laufer BI, Baca M, Foreman O, Hackos DH, Riol-Blanco L, Kaminker JS. Cross-species transcriptomic atlas of dorsal root ganglia reveals species-specific programs for sensory function. Nat Commun 2023;14:366.
[41] Ke M, Elshenawy B, Sheldon H, Arora A, Buffa FM. Single cell RNA-sequencing: a powerful yet still challenging technology to study cellular heterogeneity. BioEssays 2022;44:2200084.
[42] Klinck MP, Mogil JS, Moreau M, Lascelles BDX, Flecknell PA, Poitte T, Troncy E. Translational pain assessment: could natural animal models be the missing link? PAIN 2017;158:1633–46.
[43] Knazovicky D, Helgeson ES, Case B, Gruen ME, Maixner W, Lascelles BDX. Widespread somatosensory sensitivity in naturally occurring canine model of osteoarthritis. PAIN 2016;157:1325–32.
[44] Kol A, Arzi B, Athanasiou KA, Farmer DL, Nolta JA, Rebhun RB, Chen X, Griffiths LG, Verstraete FJM, Murphy CJ, Borjesson DL. Companion animals: translational scientist's new best friends. Sci Translat Med 2015;7:308ps21.
[45] Krauter D, Kupari J, Usoskin D, Su J, Hu Y, Zhang M-D, Ernfors P. Spatial organization, chromatin accessibility and gene-regulatory programs defining mouse sensory neurons. Commun Biol 2025;8:908.

Copyright © 2026 by the International Association for the Study of Pain. Unauthorized reproduction of this article is prohibited.

[46] Kuhn TM, Paulsen M, Cuylen-Haering S. Accessible high-speed image-activated cell sorting. Trends Cell Biol 2024;34:657–70.
[47] Kupari J, Usoskin D, Parisien M, Lou D, Hu Y, Fatt M, Lönnerberg P, Spångberg M, Eriksson B, Barkas N, Kharchenko PV, Loré K, Khoury S, Diatchenko L, Ernfors P. Single cell transcriptomics of primate sensory neurons identifies cell types associated with chronic pain. Nat Commun 2021;12:1510.
[48] Lascelles BDX, Brown DC, Maixner W, Mogil JS. Spontaneous painful disease in companion animals can facilitate the development of chronic pain therapies for humans. Osteoarthritis Cartilage 2018;26:175–83.
[49] Lascelles BDX, Brown DC, Conzemius MG, Gill M, Oshinsky ML, Sharkey M. Measurement of chronic pain in companion animals: discussions from the Pain in Animals Workshop (PAW) 2017. Vet J 2019;250:71–8.
[50] Li Y, Ji R-R. Gene therapy for chronic pain management. Cell Rep Med 2024;5:101756.
[51] Li C-L, Li K-C, Wu D, Chen Y, Luo H, Zhao J-R, Wang S-S, Sun M-M, Lu Y-J, Zhong Y-Q, Hu X-Y, Hou R, Zhou B-B, Bao L, Xiao H-S, Zhang X. Somatosensory neuron types identified by high-coverage single-cell RNA-sequencing and functional heterogeneity. Cell Res 2016;26:83–102.
[52] Lu T, Wang M, Zhou W, Ni Q, Yue Y, Wang W, Shi Y, Liu Z, Li C, Hong B, Zhou X, Zhong S, Wang K, Zeng B, Zhang J, Wang W, Zhang X, Wu Q, Wang X. Decoding transcriptional identity in developing human sensory neurons and organoid modeling. Cell 2024;187:7374–93.e28.
[53] Middleton SJ, Barry AM, Comini M, Li Y, Ray PR, Shiers S, Themistocleous AC, Uhelski ML, Yang X, Dougherty PM, Price TJ, Bennett DL. Studying human nociceptors: from fundamentals to clinic. Brain 2021;144:1312–35.
[54] Mishra SK, Hoon MA. The cells and circuitry for itch responses in mice. Science 2013;340:968–71.
[55] Nederveld SM, Krautmann MJ, Mitchell J. Safety of the selective JAK1 inhibitor oclacitinib in dogs. J Vet Pharmacol Ther 2025;48:135–45.
[56] Nguyen MQ, Wu Y, Bonilla LS, von Buchholtz LJ, Ryba NJP. Diversity amongst trigeminal neurons revealed by high throughput single cell sequencing. PLoS One 2017;12:e0185543.
[57] Nguyen MQ, von Buchholtz LJ, Reker AN, Ryba NJ, Davidson S. Single-nucleus transcriptomic analysis of human dorsal root ganglion neurons. Elife 2021;10:e71752.
[58] Pendleton AL, Shen F, Taravella AM, Emery S, Veeramah KR, Boyko AR, Kidd JM. Comparison of village dog and wolf genomes highlights the role of the neural crest in dog domestication. BMC Biol 2018;16:64.
[59] Perez-Sanchez J, Middleton SJ, Pattison LA, Hilton H, Ali Awadelkareem M, Zuberi SR, Renke MB, Hu H, Yang X, Clark AJ, St John Smith E, Bennett DL. A humanized chemogenetic system inhibits murine pain-related behavior and hyperactivity in human sensory neurons. Sci Transl Med 2023;15:eadh3839.
[60] Qi L, Iskols M, Shi D, Reddy P, Walker C, Lezgiyeva K, Voisin T, Pawlak M, Kuchroo VK, Chiu IM, Ginty DD, Sharma N. A mouse DRG genetic toolkit reveals morphological and physiological diversity of somatosensory neuron subtypes. Cell 2024;187:1508–26.e16.
[61] Renthal W, Tochitsky I, Yang L, Cheng Y-C, Li E, Kawaguchi R, Geschwind DH, Woolf CJ. Transcriptional reprogramming of distinct peripheral sensory neuron subtypes after axonal injury. Neuron 2020;108:128–44.e9.
[62] Rodrigues OR, Monard S. A rapid method to verify single-cell deposition setup for cell sorters. Cytometry A 2016;89:594–600.
[63] Ruiz Daniels R, Taylor RS, Dobie R, Salisbury S, Furniss JJ, Clark E, Macqueen DJ, Robledo D. A versatile nuclei extraction protocol for single nucleus sequencing in non-model species–optimization in various Atlantic salmon tissues. PLoS One 2023;18:e0285020.
[64] Ruzicka T, Hanifin JM, Furue M, Pulka G, Mlynarczyk I, Wollenberg A, Galus R, Etoh T, Mihara R, Yoshida H, Stewart J, Kabashima K. Anti–Interleukin-31 receptor A antibody for atopic dermatitis. N Engl J Med 2017;376:826–35.
[65] Sadler KE, Mogil JS, Stucky CL. Innovations and advances in modelling and measuring pain in animals. Nat Rev Neurosci 2022;23:70–85.
[66] Sapio MR, King DM, Maric D, Shah SR, Talbot TL, Manalo AP, Nara P, Ma W, Ghetti A, Ramsden CE, Iadarola MJ, Mannes AJ. Efficient removal of naturally-occurring lipofuscin autofluorescence in human nervous tissue using high-intensity white light. J Pain 2025;30:105359.
[67] Sharma N, Flaherty K, Lezgiyeva K, Wagner DE, Klein AM, Ginty DD. The emergence of transcriptional identity in somatosensory neurons. Nature 2020;577:392–8.
[68] Shiers S, Klein RM, Price TJ. Quantitative differences in neuronal subpopulations between mouse and human dorsal root ganglia demonstrated with RNAscope in situ hybridization. PAIN 2020;161:2410–24.
[69] Shiers SI, Sankaranarayanan I, Jeevakumar V, Cervantes A, Reese JC, Price TJ. Convergence of peptidergic and non-peptidergic protein markers in the human dorsal root ganglion and spinal dorsal horn. J Comp Neurol 2021;529:2771–88.
[70] Smith AF, Plumb AN, Berardi G, Sluka KA. Sex differences in the transition to chronic pain. J Clin Invest 2025;135:e191931.
[71] Smith ESJ, Burton MD, Heegaard A-M, Stucky CL. Not just neurons: pain is orchestrated in partnership with many non-neuronal cells. J Neurosci 2025;45:e1309252025.
[72] Snider WD, McMahon SB. Tackling pain at the source: new ideas about nociceptors. Neuron 1998;20:629–32.
[73] SynGO—Synaptic Gene Ontologies. Annotations and protein interactions. Available at: https://www.syngoportal.org/. Accessed March 31, 2026.
[74] Szőke É, Bálint M, Hetényi C, Markovics A, Elekes K, Pozsgai G, Szűts T, Kéri G, Őrfi L, Sándor Z, Szolcsányi J, Pintér E, Helyes Z. Small molecule somatostatin receptor subtype 4 (sst4) agonists are novel anti-inflammatory and analgesic drug candidates. Neuropharmacology 2020;178:108198.
[75] Tavares-Ferreira D, Shiers S, Ray PR, Wangzhou A, Jeevakumar V, Sankaranarayanan I, Cervantes AM, Reese JC, Chamessian A, Copits BA, Dougherty PM, Gereau RW, Burton MD, Dussor G, Price TJ. Spatial transcriptomics of dorsal root ganglia identifies molecular signatures of human nociceptors. Sci Transl Med 2022;14:eabj8186.
[76] The human transcription factors. Available at: https://humantfs.ccbr.utoronto.ca/. Accessed March 31, 2026.
[77] Todd AJ. Neuronal circuitry for pain processing in the dorsal horn. Nat Rev Neurosci 2010;11:823–36.
[78] Usoskin D, Furlan A, Islam S, Abdo H, Lönnerberg P, Lou D, Hjerling-Leffler J, Haeggström J, Kharchenko O, Kharchenko PV, Linnarsson S, Ernfors P. Unbiased classification of sensory neuron types by large-scale single-cell RNA sequencing. Nat Neurosci 2015;18:145–53.
[79] Van Brussel L, Moyaert H, Escalada M, Mahabir SP, Stegemann MR. A masked, randomised clinical trial evaluating the efficacy and safety of lokivetmab compared to saline control in client-owned dogs with allergic dermatitis. Vet Dermatol 2021;32:477.
[80] Vonholdt BM, Pollinger JP, Lohmueller KE, Han E, Parker HG, Quignon P, Degenhardt JD, Boyko AR, Earl DA, Auton A, Reynolds A, Bryc K, Brisbin A, Knowles JC, Mosher DS, Spady TC, Elkahloun A, Geffen E, Pilot M, Jedrzejewski W, Greco C, Randi E, Bannasch D, Wilton A, Shearman J, Musiani M, Cargill M, Jones PG, Qian Z, Huang W, Ding Z-L, Zhang Y-P, Bustamante CD, Ostrander EA, Novembre J, Wayne RK. Genome-wide SNP and haplotype analyses reveal a rich history underlying dog domestication. Nature 2010;464:898–902.
[81] Wang G-D, Shao X-J, Bai B, Wang J, Wang X, Cao X, Liu Y-H, Wang X, Yin T-T, Zhang S-J, Lu Y, Wang Z, Wang L, Zhao W, Zhang B, Ruan J, Zhang Y-P. Structural variation during dog domestication: insights from gray wolf and dhole genomes. Natl Sci Rev 2019;6:110–22.
[82] Wang Q, Zhao G, Ding H, Wang Z, Wu J, Huang H, Cao L, Wang H, Gao Z, Feng J. Trpv1-lineage neuron-expressing Kcnq4 channel modulates itch sensation in mice. PAIN 2024;166:1475–86.
[83] Weir GA, Middleton SJ, Clark AJ, Daniel T, Khovanov N, McMahon SB, Bennett DL. Using an engineered glutamate-gated chloride channel to silence sensory neurons and treat neuropathic pain at the source. Brain 2017;140:2570–85.
[84] Wu Z, Wang Y, Chen W, Sun H, Chen X, Li X, Wang Z, Liang W, Wang S-Y, Luan X, Li Y, Huang S, Liang Y, Zhang J, Chen Z-F, Wang G, Gao Y, Liu Y, Wang J, Liu Z, Shi P, Liu C, Lv L, Hou A, Wu C, Yao C, Hong Z, Dai J, Lu Z, Pan F, Chen X, Kettenmann H, Amit I, Speakman JR, Chen Y, Ginhoux F, Cui R, Huang T, Li H. Peripheral nervous system microglia-like cells regulate neuronal soma size throughout evolution. Cell 2025;188:2159–74.e15.
[85] Yu H, Nagi SS, Usoskin D, Hu Y, Kupari J, Bouchatta O, Yan H, Cranfill SL, Gautam M, Su Y, Lu Y, Wymer J, Glanz M, Albrecht P, Song H, Ming G-L, Prouty S, Seykora J, Wu H, Ma M, Marshall A, Rice FL, Li M, Olausson H, Ernfors P, Luo W. Leveraging deep single-soma RNA sequencing to explore the neural basis of human somatosensation. Nat Neurosci 2024;27:2326–40.
[86] Zeisel A, Hochgerner H, Lönnerberg P, Johnsson A, Memic F, van der Zwan J, Häring M, Braun E, Borm LE, La Manno G, Codeluppi S, Furlan A, Lee K, Skene N, Harris KD, Hjerling-Leffler J, Arenas E, Ernfors P, Marklund U, Linnarsson S. Molecular architecture of the mouse nervous system. Cell 2018;174:999–1014.e22.
[87] Zeng X, Martinez-Garcia RI, Bhuiyan SA, Heo K, MacKinnon-Booth N, Bentley E, Shea E, Wu K, Barkai O, Turnes BL, Jayakar SS, Gomez-Eslava B, Hameed MQ, Santiago C, Lezgiyeva K, Osei-Asante E, Furfaro I, Rotenberg A, Johnston BR, Wainger BJ, Renthal W, Lacour SP, Ginty DD, Woolf CJ. Injured SSTR2 + nociceptor axons in neuromas drive chronic spontaneous neuropathic pain. bioRxiv. 2025. https://doi.org/10.1101/2025.09.30.679489.
[88] Zhao G, Boyer K, Meriau P, Yang L, Naz H, Rosen S, Murray G, Dourson A, Mwirigi J, Del Rosario J, Payne M, Gupta P, Yi J, Slivicki R, Bertels Z,

Copyright © 2026 by the International Association for the Study of Pain. Unauthorized reproduction of this article is prohibited.

Lemen J, Chen Y, Wang T, Chamessian A, Copits BA, Gereau RW, Cavalli V. Single nucleus multiomic atlas of human dorsal root ganglia reveals the contribution of non-neuronal cell types to pain. bioRxiv 2025. doi: 10.1101/2025.09.21.677655

[89] Zhou Q-J, Liu X, Zhang L, Wang R, Yin T, Li X, Li G, He Y, Ding Z, Ma P, Wang S-Z, Mao B, Zhang S, Wang G-D. A single-nucleus transcriptomic atlas of the dog hippocampus reveals the potential relationship between specific cell types and domestication. Natl Sci Rev 2022;9:nwac147.

Copyright © 2026 by the International Association for the Study of Pain. Unauthorized reproduction of this article is prohibited.